Inflationary Spectral Indices and Potential Reconstruction

Loison Hoi

Master of Science

Department of Physics

McGill University

Montréal, Québec, Canada

September 14, 2006

A thesis submitted to McGill University

in partial fulfillment of the requirements of the degree of Master of Science

Copyright © Loison Hoi, 2006

Library and Archives Canada

Published Heritage Branch

395 Wellington Street
Ottawa ON K1A 0N4
Canada

Bibliothèque et Archives Canada

Direction du Patrimoine de l'édition

395, rue Wellington
Ottawa ON K1A 0N4
Canada

Your file Votre référence
ISBN: 978-0-494-28494-0
Our file Notre référence
ISBN: 978-0-494-28494-0

NOTICE:
The author has granted a non-exclusive license allowing Library and Archives Canada to reproduce, publish, archive, preserve, conserve, communicate to the public by telecommunication or on the Internet, loan, distribute and sell theses worldwide, for commercial or non-commercial purposes, in microform, paper, electronic and/or any other formats.

The author retains copyright ownership and moral rights in this thesis. Neither the thesis nor substantial extracts from it may be printed or otherwise reproduced without the author's permission.

AVIS:
L'auteur a accordé une licence non exclusive permettant à la Bibliothèque et Archives Canada de reproduire, publier, archiver, sauvegarder, conserver, transmettre au public par télécommunication ou par l'Internet, prêter, distribuer et vendre des thèses partout dans le monde, à des fins commerciales ou autres, sur support microforme, papier, électronique et/ou autres formats.

L'auteur conserve la propriété du droit d'auteur et des droits moraux qui protège cette thèse. Ni la thèse ni des extraits substantiels de celle-ci ne doivent être imprimés ou autrement reproduits sans son autorisation.

In compliance with the Canadian Privacy Act some supporting forms may have been removed from this thesis.

While these forms may be included in the document page count, their removal does not represent any loss of content from the thesis.

Conformément à la loi canadienne sur la protection de la vie privée, quelques formulaires secondaires ont été enlevés de cette thèse.

Bien que ces formulaires aient inclus dans la pagination, il n'y aura aucun contenu manquant.

Canada

Abstract

The Inflationary power spectrum plays an important role in modern cosmology. In this thesis, we studied both the experimental and theoretical aspects of the inflationary spectral index. By exploring the recent WMAP data, we found that the evidence for the running of the spectral index mainly comes from multipoles near $l = 40$. This fact allows a partial running spectrum to give as good a fit as the WMAP running spectrum. We gave some simple formulae for the inflationary spectral indices based on the Hamilton-Jacobi formulation of inflation. These simple formulae agree with the exact solutions in some special cases. The Hamilton-Jacobi formulation of inflation was also applied to reconstruct inflaton potentials from a given power spectrum. A simple and accurate reconstruction formulation was presented. All analytic potentials giving a constant spectral index are derived, which show that a nearly scale-invariant spectrum can give rise to slow-roll inflation during 60 e-foldings within sub-Planckian inflaton field values and a potential energy $V^{1/4} \sim 10^{15}$GeV. Potentials for large running of the spectral index and large tensor-to-scalar ratio were also constructed, which need super-Planckian field values and require that the slow-roll approximation breaks down before reaching 60 e-foldings. We have shown that for the cosmologically interesting scales, a renormalizable potential fits the reconstructed potential for a large running spectrum very well. Our reconstruction formulation also produces a self-consistent tensor spectrum once a scalar spectrum and the tensor-to-scalar ratio are given. Higher order corrections to the slow-roll approximation are also considered. We showed that they can be incorporated straightforwardly into our formulae for spectral indices and the reconstruction formalism.

Résumé

Le spectre de puissance inflationniste joue un rôle important en cosmologie moderne. Dans cette thèse, nous étudions les aspects expérimentaux et théoriques de l'indice spectral inflationniste. En étudiant les données récentes de WMAP, nous trouvons que les évidences de la variation de l'indice spectral provient principalement des multipôles près de $l = 40$. Ceci permet au spectre partiel variable de présenter une aussi bonne concordance que le spectre WMAP variable. Nous présentons des formules simples pour les indices spectraux inflationniste basées sur la formulation Hamilton-Jacobi de l'inflation. Ces formules simples sont en accord avec les solutions exactes dans certains cas simples. La formulation Hamilton-Jacobi de l'inflation est aussi appliquée à la reconstruction de potentiels inflationnistes à partir du spectre de puissance. Une formulation de reconstruction simple et précise est présentée. Tous les potentiels analytiques pour un indice spectral constant sont dérivés, montrant ainsi qu'un spectre presque invariant d'echelle peut produire de l'inflation avec roulement lent pendant 60 e-repliements avec des valeurs de champ d'inflaton sub-Planckienne d'énergie potentielle $V^{1/4} \sim 10^{15}$ GeV. Des potentiels avec une variation de l'indice spectral et un ratio tenseur-sur-scalaire élevés sont aussi construits; ceux-ci ont besoins de valeurs de champ super-Planckiennes et l'approximation du roulement lent devient invalide avant d'atteindre 60 e-repliements. Nous montrons que pour des échelles intéressantes cosmologiquement, un potentiel renormalisable et le potentiel reconstruit concordent bien pour une grande variation du spectre. Notre formulation de reconstruction produit aussi un spectre tensoriel auto-consistant dans la mesure où un spectre scalaire et un ratio tenseur-sur-scalaire sont donnés. Des corrections d'ordre supérieures à l'approximation du roulement lent sont aussi considérées. Nous montrons qu'elles peuvent être incorporées directement dans nos formules pour l'indice spectral et nos formules de reconstruction.

Acknowledgements

First, I am grateful to my supervisor, Professor James Cline, for his patience, encouragement, and supervision during my Master program, and for many helpful discussion and comments on the manuscript of this thesis.

I would like to thank Aaron Berndsen for his review of this thesis and the translation of the French abstract. I thank Professor Gilbert Holder for his help with using CosmoMC. I acknowledge the thesis committee for sharing their time, expertise, and advice.

I am thankful to Professor Robert Brandenberger and Professor Guy Moore, who gave inspiring lectures on cosmology and particle physics. Thanks to my colleagues in Physics Department. It is a pleasure to learn, study, and work with them. I also would like to express my appreciation to my friends who help me enjoy my life in Montreal.

I thank Department of Physics, McGill University, for the financial support, and the Tertiary Education Services Office, Macau SAR, for the postgraduate scholarship for my Master program.

Finally, I would like to express my gratitude to my parents who are always supportive to my career, and I am grateful to my older brother for his understanding and support to our family.

Contents

1 Introduction **1**

1.1 Standard Cosmology 1

1.2 Inflationary Cosmology 4

1.3 Primordial Power Spectra 6

2 WMAP Power Spectrum **9**

2.1 Nearly Scale-Invariant Spectrum 9

2.2 Large Running Power Spectrum 15

3 Inflationary Spectral Index **27**

3.1 Hamilton-Jacobi Formulation of Inflation 27

3.2 Inflationary Spectral Indices 29

3.3 Corrections to the Spectral Indices 30

4 Reconstruction of Inflaton Potentials **33**

4.1 Reconstruction Formulation 33

4.2 Corrections to the Reconstruction Formulation 36

4.3 Inflationary Attractor 39

5 Reconstruction: Constant Spectral Index **41**

5.1 Particular Potentials 41

5.2 General Solutions 47

5.3 Summary of Constant Spectral Index 54

6 Reconstruction: Running Spectral Index **59**

6.1 Unique Solution? 59

6.2 Tensor Spectrum 62

6.3 WMAP Running Power Spectrum 64

7 Conclusions **73**

A Units and Constants **75**

Bibliography **76**

List of Tables

2.1 Best fit non-running models for the first year and three-year WMAP data. 11
2.2 Best fit non-running models for the combinations of the first year WMAP and other data sets. 13
2.3 Best fit non-running models for the combinations of the three-year WMAP and other data sets. 14
2.4 Best fit running models for the first year and three-year WMAP data. 20
2.5 Best fit running models for the combinations of the first year WMAP and other data sets. 21
2.6 Best fit running models for the combinations of the three-year WMAP and other data sets. 22

List of Figures

2.1 The parameter distributions for the non-running model using the three-year WMAP data. 16

2.2 The spectral index n_s as a function of k for the combination of the first year WMAP and other data. 17

2.3 The parameter distributions for the running model using the three-year WMAP data. 19

2.4 The best fit power spectra of the first year WMAP data. 23

2.5 The best fit power spectra of the three-year WMAP data. 24

2.6 Difference of χ^2 between the best fit non-running and running models of the first year WMAP data, versus the minimum multipole included $l_{\rm min}$. The separate contributions from temperature (TT) and polarization (TE) as well as the total are shown. 25

2.7 Difference of χ^2 between the best fit non-running and running models of the three-year WMAP data, versus the minimum multipole included $l_{\rm min}$. The separate contributions from temperature (TT) and polarization (TE) as well as the total are shown. 26

4.1 The first and second order reconstructed power spectra for the best fit WMAP running model. 38

4.2 The first order reconstructed power spectra for the best fit WMAP running model with different initial inflaton velocities. 40

5.1 The reconstructed potential for a scale-invariant spectrum. 44

5.2 The reconstructed potential for a constant spectral index: $n = 2$. . . . 46

5.3 The reconstructed potentials for a constant spectral index: $0 < n < 2$. 49
5.4 The reconstructed potentials for a constant spectral index: $n < 0$ with $C = 1$. 51
5.5 The reconstructed potentials for a constant spectral index: $n > 2$ with $C = 1$. 52
5.6 The reconstructed potentials for a constant spectral index: $n < 0$ with $C = -1$. 53
5.7 Three potentials with $n < 0$ have the same asymptotic behaviors. . . 55
5.8 The reconstructed potential for a constant spectral index with $n = 7(> 6)$ shows that $V' = 0$ during inflation. 56

6.1 The tensor spectra reconstructed from the scalar spectrum and from the inflationary consistency equation. 64
6.2 The reconstructed Hubble parameter and inflaton potential for the best fit WMAP running model. 65
6.3 The logarithm of the scale factor as a function of time reconstructed from the best fit WMAP running model. 68
6.4 The reconstructed slow-roll parameters for the best fit WMAP running model. 69
6.5 The reconstructed slow-roll parameters for the WMAP partial running model. 70
6.6 The reconstructed potential for the WMAP partial running model. . 71
6.7 The reconstructed potential for the best fit WMAP running model and a series of renormalizable potentials fitting over different ranges of field values. 71
6.8 The fractional errors of the fitting potentials. The correlation coefficient r for each fit is also shown. 72

Chapter 1

Introduction

Inflation has become an important part of modern cosmology since A. Guth's seminal paper [1], which is designed to solve the horizon and flatness problems. Moreover, inflation is the first theory which gives causal explanation to the large-scale structure of the present universe. In this chapter, we start with a brief introduction to the successes and problems of standard cosmology [2, 3], and introduce the achievements of inflationary cosmology [4, 5] with emphasis on the results of the inflationary spectral index in the slow-roll approximation [6, 7].

1.1 Standard Cosmology

The study of modern cosmology began when Einstein presented the general theory of relativity in 1915. In general relativity, spacetime and matter are connected through the spacetime metric, which not only describes the geometry of spacetime but also determines the motion of matter. In order to apply general relativity to the universe, Einstein made a convenient assumption that on large scales the universe is homogeneous, which now is referred to as the cosmological principle and confirmed by experiments. The cosmological principle leads to a homogeneous and isotropic

metric, the Robertson-Walker metric:[1]

$$ds^2 = -dt^2 + a(t)^2 \left[\frac{dr^2}{1 - Kr^2} + r^2 \left(d\theta^2 + \sin^2\theta d\varphi^2 \right) \right], \tag{1.1}$$

where spatial coordinates, (r, θ, φ), are comoving coordinates, and hence the physical distance is a product of the comoving distance and the scale factor, $a(t)$; K is the spatial curvature constant and it determines the topology of the three spatial dimensions: $K = 0$ gives a flat universe, $K > 0$ a closed (finite) universe, and $K < 0$ an open (infinite) universe.[2]

The third pillar of standard cosmology is that "matter" can be regarded as a perfect fluid; its properties are determined by its energy density $\rho(t)$ and pressure $p(t)$. The resultant Einstein field equations are

$$3H^2 = \rho + \Lambda - \frac{3K}{a^2}, \tag{1.2}$$

$$\ddot{a} = -\frac{1}{6}(\rho + 3p), \tag{1.3}$$

where overdots denote derivatives with respect to time and the reduced Planck mass, $M_{\rm Pl} = (8\pi G)^{-1/2}$, is set to 1 throughout this thesis;[3] Λ is the cosmological constant, which can be effectively regarded as vacuum energy and is absorbed into the energy density, ρ, hereafter. Eq. (1.2) is referred to as the Friedmann equation, which connects the total energy density and the Hubble parameter:

$$H(t) \equiv \frac{\dot{a}(t)}{a(t)}. \tag{1.4}$$

The Friedmann equation and the Einstein field equation, Eq. (1.3), can be combined to give the continuity equation:

$$\dot{\rho} = -3H(\rho + p). \tag{1.5}$$

[1]We use natural units throughout this thesis. See Appendix A for conversion between natural units and international units.

[2]Although the universe is also infinite if $K = 0$, the terminology "open universe" is reserved for the case of negative spatial curvature.

[3]See Appendix A.

For relativistic matter (radiation), $\rho \simeq 3p$, which gives rise to a scale factor as $a \propto t^{1/2}$; for non-relativistic matter ("dust," or just "matter"), $p \simeq 0$ and hence $a \propto t^{2/3}$. Standard cosmology gives an excellent description of the radiation and matter domination epochs, and hence a clear picture of the evolution of the universe: The universe starts with a hot, dense, and thermal equilibrium state (Big Bang); as the universe expands, the temperature decreases and the universe goes through nucleosynthesis, decoupling of photons, and formation of structure (galaxies).

The confirmation of Hubble's law, the prediction of abundances of light elements, and the Cosmic Microwave Background (CMB) are three classic tests of standard cosmology for which the big bang theory succeeds remarkable well. Moreover, the CMB provides much information about the early universe, and recent high-precision observations of the CMB anisotropy, by the Wilkinson Microwave Anisotropy Probe (WMAP), are designed to accurately determine basic cosmological parameters, such as today's Hubble parameter, the age of the universe, and the composition of the energy density of the universe [8, 9].

Despite its great successes, standard big bang cosmology does not shed light on the infant universe far before nucleosynthesis, and three critical cosmological problems are left over. Firstly, due to its expansion, today's observable universe would consist of many patches which were out of causal contact in the past, and hence there is no causal explanation for the homogeneity of the CMB; this is the horizon problem. Secondly, defining the critical density as $\rho_c = 3H^2$, and the fractional density as $\Omega = \rho/\rho_c$, the Friedmann equation can be rewritten as

$$|\Omega_{\text{tot}} - 1| = \frac{|K|}{a^2 H^2}. \tag{1.6}$$

So the deviation of the total density from unity is monotonically increasing with time in the radiation and matter domination epochs. However, today's total density is close to unity, $\Omega_{\text{tot}} = 1.02 \pm 0.02$ [11]. Therefore, a question arises: Why is the universe still so flat even though the deviation has been amplified by a factor of more than 10^{16} since nucleosynthesis? This problem is referred to as the flatness problem. The third problem is the structure formation problem. On one hand there is no causal

mechanism for the observed large-scale structure; moreover, standard cosmology does not provide a mechanism for the generation of primordial density perturbations.

1.2 Inflationary Cosmology

The idea of inflation is that a rapid expansion epoch in the early universe could solve the above cosmological problems. Specifically, we define inflation as an epoch with the comoving Hubble radius decreasing with time; from the Einstein field equation, Eq. (1.3), this definition is equivalent to an accelerating expansion epoch [6]:

$$\text{Inflation} \Longleftrightarrow \frac{d}{dt}\left(\frac{H^{-1}}{a}\right) < 0 \Longleftrightarrow \ddot{a} > 0. \tag{1.7}$$

The decrease of the comoving Hubble radius would shrink the present observable universe into a causally connected region, and hence the horizon problem could be solved. As for the flatness problem, it is obvious that the deviation of the total density from unity is suppressed during inflation. Moreover, inflation sets the early quantum fluctuations as seeds of structure formation at late times, so the structure formation problem can be solved by causal physics.

Although inflation is a brilliant idea, it is hard to achieve inflation with well-motivated particle physics theories since inflation typically requires near Planck scale physics. Nevertheless, people usually consider a class of inflationary models which is driven by a single scalar field, the inflaton field ϕ, by which the energy density and pressure are

$$\rho = \frac{1}{2}\dot{\phi}^2 + V(\phi), \tag{1.8}$$

$$p = \frac{1}{2}\dot{\phi}^2 - V(\phi), \tag{1.9}$$

where $V(\phi)$ is the inflaton potential and the spatial gradient terms are omitted since we consider a homogeneous background universe. From the Friedmann equation and the continuity equation, the equations of motion become

$$V + \frac{1}{2}\dot{\phi}^2 = 3H^2, \tag{1.10}$$

$$\ddot{\phi} + 3H\dot{\phi} = -V', \tag{1.11}$$

where primes denote derivatives with respect to the inflaton field; the spatial curvature term is dropped hereafter since we consider a flat universe only. An accelerating epoch requires that the potential energy dominates, $V > \dot{\phi}^2$. Generally, a generic inflation model, deemed slow-roll inflation, is usually employed. In this scenario the inflaton field slowly rolls and the potential energy dominates until the end of inflation:

$$3H^2 \simeq V, \tag{1.12}$$

$$3H\dot{\phi} \simeq -V'. \tag{1.13}$$

The satisfaction of the above slow-roll approximation is quantified by the magnitude of the slow-roll parameters [10]:

$$\epsilon_{\rm V} \equiv \frac{1}{2}\left(\frac{V'}{V}\right)^2, \tag{1.14}$$

$$\eta_{\rm V} \equiv \frac{V''}{V}, \tag{1.15}$$

with

$$\epsilon_{\rm V} \ll 1, \tag{1.16}$$

$$|\eta_{\rm V}| \ll 1. \tag{1.17}$$

Therefore, the end of inflation is indicated by $\epsilon_{\rm V} \simeq 1$ or $|\eta_{\rm V} \simeq 1|$. Note that these conditions are not sufficient for the slow-roll approximation to be valid because they only restrict the shape of the potential but not the dynamics; an attractor behavior of the solutions is required for the slow-roll approximation to be valid. We use a rigorous treatment of the equations of motion in this thesis; see Chapter 3. Also see Section 4.3 for a discussion about the inflationary attractor.

The amount of inflation can be expressed through the number of e-foldings from time t to the end of inflation:

$$N(t) \equiv \ln\frac{a_{\rm end}}{a(t)} = \int_t^{t_{\rm end}} H(t)dt. \tag{1.18}$$

In the slow-roll approximation, it can be expressed as

$$N \simeq \int_{\phi_{\rm end}}^{\phi} \frac{V}{V'}d\phi. \tag{1.19}$$

Typically, 60 e-foldings are needed for today's observable universe to solve the cosmological problems. Differentiating the above expression, one has the relation between the inflaton field and the number of e-foldings:

$$\frac{d\phi}{dN} \simeq \frac{V'}{V}. \tag{1.20}$$

1.3 Primordial Power Spectra

One of the features of inflation is that it relates the present large-scale structure to the small fluctuations in the early universe. The idea is that vacuum fluctuations of the inflaton field, $\delta\phi$, occur during inflation, which give rise to resultant density fluctuations and metric fluctuations. During inflation, these fluctuations are stretched well outside the horizon, where they are frozen for a long cosmic time. Well after nucleosynthesis, cosmologically interesting scales begin to reenter the horizon, and that is the initial epoch for structure formation. The initial power spectrum is observable today; therefore it provides an important test of inflationary cosmology.

The details of the cosmological perturbation theory are beyond the scope of this thesis; the results, however, are simple and crucial for the discussion of the remaining chapters. The power spectra of the primordial curvature perturbation ($\mathcal{R}$; also referred to as the power spectrum of scalar field perturbation) and gravitational waves (h; also referred to as the spectrum of tensor modes perturbation) are

$$\mathcal{P}_{\mathcal{R}}(k) = \left(\frac{H}{2\pi}\right)^2 \left(\frac{H}{\dot{\phi}}\right)^2 \Bigg|_{k=aH}, \tag{1.21}$$

$$\mathcal{P}_h(k) = 8\left(\frac{H}{2\pi}\right)^2 \Bigg|_{k=aH}, \tag{1.22}$$

where the relation of the inflaton field, ϕ, and the comoving wavenumber, k, is given implicitly through the horizon crossing condition,

$$k = aH, \tag{1.23}$$

which will not be written down explicitly in equations hereafter; a factor of 8 in $\mathcal{P}_h$ is introduced to be consistent with conventions of the WMAP collaboration [11, 12, 13].

Eqs. (1.21) and (1.22) are the leading order results of slow-roll inflation; the next order results are discussed in Sections 3.3 and 4.2. Besides, we discuss only single-field inflation in this thesis. Since gravitational waves couple to matter fluctuations weakly, the effect of the CMB anisotropy is dominated by the scalar field, and we mainly discuss the curvature perturbation spectrum in this thesis.

The curvature perturbation is usually parameterized as a phenomenological power-law spectrum:

$$\mathcal{P}_{\mathcal{R}} = \mathcal{P}_{\mathcal{R}0} \left(\frac{k}{k_0} \right)^{n_s - 1}, \tag{1.24}$$

where k_0 is a chosen pivot point and $\mathcal{P}_{\mathcal{R}0}$ is the corresponding normalization; the number -1 in the exponent comes from a historical convention. This parameterization can be easily generalized to the definitions of the spectral indices for scalar and tensor spectra:

$$n_s - 1 \equiv \frac{d \ln \mathcal{P}_{\mathcal{R}}}{d \ln k}, \tag{1.25}$$

$$n_t \equiv \frac{d \ln \mathcal{P}_h}{d \ln k}. \tag{1.26}$$

Since fluctuations are stretched outside the horizon rapidly by inflation, differences between different modes are expected to be small; as a result, the power spectra should be close to scale-invariant spectra, *i.e.* $n_s \simeq 1$ and $n_t \simeq 0$.

For slow-roll inflation, the expressions for the spectra can be simplified to

$$\mathcal{P}_{\mathcal{R}}(k) \simeq \frac{1}{12\pi^2} \frac{V^3}{V'^2}, \tag{1.27}$$

$$\mathcal{P}_h(k) \simeq \frac{2}{3\pi^2} V, \tag{1.28}$$

and differentiating the relation of horizon crossing condition approximately gives

$$d \ln k \simeq dN, \tag{1.29}$$

due to the fact that the Hubble parameter hardly changes during slow-roll inflation. The spectral indices are obtained straightforwardly in terms of the slow-roll parameters (Eqs. (1.14) and (1.15)) [10]:

$$n_s - 1 \simeq -6\epsilon_{\mathrm{V}} + 2\eta_{\mathrm{V}}, \tag{1.30}$$

$$n_t \simeq -2\epsilon_{\mathrm{V}}. \tag{1.31}$$

The spectral indices are not constants in general. Their runnings are defined as

$$\alpha_s \equiv \frac{dn_s}{d\ln k}, \tag{1.32}$$

$$\alpha_t \equiv \frac{dn_t}{d\ln k}. \tag{1.33}$$

The slow-roll predictions are [14]

$$\alpha_s \simeq -24\epsilon_{\rm V}^2 + 16\epsilon_{\rm V}\eta_{\rm V} - 2\xi_{\rm V}, \tag{1.34}$$

$$\alpha_t \simeq 4\epsilon_{\rm V}(\eta_{\rm V} - 2\epsilon_{\rm V}), \tag{1.35}$$

where $\xi_{\rm V}$ is the third slow-roll parameter [15]:

$$\xi_{\rm V} \equiv \frac{V'}{V}\frac{V''}{V}. \tag{1.36}$$

Since the runnings are of order $O(\epsilon_{\rm V}^2)$, their effects are expected to be small.

The tensor-to-scalar ratio is defined as

$$r \equiv \frac{\mathcal{P}_h}{\mathcal{P}_{\mathcal{R}}}. \tag{1.37}$$

In terms of the slow-roll parameters, it is

$$r(k) \simeq 16\epsilon_{\rm V}(k). \tag{1.38}$$

Thus the tensor spectral index can be approximately expressed as

$$n_t \simeq -\frac{r}{8}, \tag{1.39}$$

which is referred to as the inflationary consistency equation [14].

The scalar and tensor power spectra can be inferred from the CMB anisotropy, thus they provide indirect tests to inflationary cosmology. Nevertheless, the inverse problem, "what is the shape of the inflaton potential for a given power spectrum?" has not been solved accurately. In the following chapters, we first reexamine the experimental evidence for the scalar power spectrum; then we use a rigorous treatment of the inflaton equations of motion and give more accurate formulae for the spectral indices. We present a simple and accurate method for the reconstruction of inflaton potentials in Chapter 4. This general reconstruction formulation is implemented in the cases of constant and running spectral index in Chapters 5 and 6, where experimental results are applied and thus constraints on inflationary cosmology arise. We give conclusions in Chapter 7.

Chapter 2

WMAP Power Spectrum

The WMAP mission was designed to precisely detect the tiny fluctuations in the CMB and thus accurately determine the basic cosmological parameters. It was launched in 2001, and the first year and three-year data were released in 2003 and 2006 respectively. In this chapter, we explore the experimental evidence for the primordial power spectrum from WMAP and other up-to-date astrophysical data.

2.1 Nearly Scale-Invariant Spectrum

Consider a simple and basic cosmological model: a flat universe filled with radiation, baryons, cold dark matter, and a cosmological constant, where the primordial power spectrum can be parameterized with a power-law spectrum. This model is referred to as the ΛCDM model (to distinguish from the running spectral index model introducted in the next section, we also call it the non-running model), and it is described by six basic parameters: the scalar spectral index n_s, the normalization parameter of the power spectrum A, the optical depth to the decoupling surface τ, today's Hubble constant h (in units of 100km/s/Mpc), the baryon density $\Omega_b h^2$, and the matter density $\Omega_m h^2$. This model fits both the first year and three-year WMAP data very well; moreover, it is consistent with the predictions given by inflation–a flat universe, gaussian primordial fluctuations, and a nearly scale-invariant spectrum [11, 13].

We reexamined the ΛCDM model using CosmoMC, a Markov-Chain Monte-Carlo

engine for exploring cosmological parameter space [16].[1] Table 2.1 lists our best fit values for the cosmological parameters and also quotes the best fit parameters given by the WMAP collaboration [11, 13]. One should be aware of the difference between the best fit model (values) and the marginalized (mean) values. A marginalized value is a 1-dimensional expectation value by marginalizing over all other parameters; it and its uncertainty usually represent the best estimate for a single parameter. The best fit model is one point in the parameter space minimizing $\chi^2 = -2\ln\mathcal{L}$, where $\mathcal{L}$ is the likelihood function; its uncertainties depend on the likelihood surface and are usually complicated and not shown. It is obvious that the combination of all marginalized values does not necessarily give the best fit model. If one considers more than one parameter at the same time, the best fit model is preferred; for example, the best fit CMB angular spectra are given through the best fit model, not the marginalized values. Values in this thesis are from best fit models unless specified.

To search a best fit point, we usually set $\Delta\ln\mathcal{L} < 0.05$, so the tolerance on χ^2 is less than 0.1. However, we have observed that there is a tendency for CosmoMC to get stuck in local minima of χ^2 when searching for best fit points, and hence it is possible that the values listed in this chapter are not the global minima. To alleviate this problem, we tried to start with different regions in the parameter space. Besides, Markov Chains also provide the best fit points among the accepted samples. Nevertheless, we will show how the parameters and claims change if one falls in a local minimum.

CosmoMC uses $(\Omega_c h^2, 100\theta, \ln[10^{10}\mathcal{P}_{\mathcal{R}0}])$ instead of $(\Omega_m h^2, h, A)$. The relation between the cold dark matter density $\Omega_c h^2$ and the matter density density $\Omega_m h^2$ is $\Omega_m h^2 = \Omega_c h^2 + \Omega_b h^2$. θ is the ratio of the sound horizon to the angular diameter distance, and it indicates the position of the first peak of the CMB temperature angular spectrum; the values of θ's are also shown in the table.[2] The relation between

[1]See http://www.cosmologist.info/cosmomc. The author thanks Antony Lewis for help with using CosmoMC.

[2]We discuss only the parameters directly related to the scalar and tensor power spectra in this thesis; see, *e.g.*, Refs. [2, 3, 6] for discussion about the CMB angular spectrum and other cosmological

Table 2.1: Best fit non-running models for the first year and three-year WMAP data.

Parameter	WMAP1 [11]	WMAP1a	WMAP1b	WMAP3 [13]	WMAP3a
n_s	0.97	0.96	0.99	0.96	0.95
A	0.86^a	0.87	0.88	$-^c$	0.81
τ	0.10	0.11	0.16	0.092	0.090
h	0.68	0.69	0.72	0.73	0.73
$100\Omega_b h^2$	2.3	2.29	2.36	2.22	2.22
$\Omega_m h^2$	0.145^b	0.145	0.140	0.128	0.128
100θ	–	1.045	1.047	–	1.040
χ^2	1431	1428.8	1429.5	–	11252.3
ν	1342	1342	1342	–	–

[a]The original value is $A(0.05) = 0.78$. Here we take $n_s = 0.97$ to evaluate $A(0.002)$.

[b]This is the value from Ref. [13]; the value given by Ref. [11] is 0.13.

[c]Ref. [13] uses the amplitude of galaxy fluctuations instead of the normalization parameter A; its value is $\sigma_8 = 0.77$.

$\mathcal{P}_{\mathcal{R}0}$ and A is [12]

$$\mathcal{P}_{\mathcal{R}0} = \frac{2 \times 10^4 \pi^2}{9 T_{\rm CMB}^2} A \simeq 2.95 \times 10^{-9} A, \tag{2.1}$$

where $T_{\rm CMB} = 2.725 \times 10^6 \mu K$. We choose the pivot point $k_0 = 0.002 {\rm Mpc}^{-1}$ throughout this thesis; for other pivot point values, one has

$$\begin{aligned} \ln \mathcal{P}_{\mathcal{R}}(k) &= \ln \mathcal{P}_{\mathcal{R}0}(k_0) + [n_s(k_0) - 1] \ln \frac{k}{k_0} + \frac{1}{2}\alpha_s(k_0) \ln^2 \frac{k}{k_0} \qquad (2.2) \\ &= \left\{ \ln \mathcal{P}_{\mathcal{R}0}(k_0) + [n_s(k_0) - 1] \ln \frac{k_0'}{k_0} + \frac{1}{2}\alpha_s(k_0) \ln^2 \frac{k_0'}{k_0} \right\} \\ &\quad + \left[n_s(k_0) - 1 + \alpha_s(k_0) \ln \frac{k_0'}{k_0} \right] \ln \frac{k}{k_0'} + \frac{1}{2}\alpha_s(k_0) \ln^2 \frac{k}{k_0'}. \qquad (2.3) \end{aligned}$$

In Table 2.1, the number of degrees of freedom, ν, is the number of data points minus the number of parameters. For the first year WMAP data, there are 899 data points for the TT spectrum ($l = 2 - 900$, l is the multipole of the CMB angular

parameters.

spectrum), and 449 for the TE spectrum ($l = 2-450$). Therefore, $\nu = 899+449-6 = 1342$, and the reduced χ^2, χ^2/ν, is 1.065. The three-year WMAP data mixes the C_l likelihoods for high multipoles ($l = 13 - 1000$ for TT, $l = 24 - 450$ for TE) and the pixel likelihoods for low multipoles ($l = 2 - 12$ for TT, $l = 2 - 23$ for TE), so the values of χ^2 and ν do not have absolute meanings.

The first column of Table 2.1 is the best fit model for the first year WMAP data [11]; it is consistent with a nearly scale-invariant spectrum as predicted by slow-roll inflation. The second column (1a) lists our best fit model, which is consistent with the best fit model given by the WMAP collaboration [11]. The fact that these two columns are not identical may be due to different settings; for example, the maximum l in the calculation of the likelihood.[3] We found another "best fit" point in the first year data, which has an almost scale-invariant spectral index and a relatively high optical depth, as shown in the third column (1b) of Table 2.1. Compared to column 1a, the model in column 1b is obvious a local minimum. This is due to the fact that there is a long, flat degeneracy between n_s and τ in the first year WMAP data [11]. The three-year data, however, breaks this degeneracy with the help of the polarization data [17]. It turns out that the best fit model favors a spectral index less than the scale-invariant value and a lower optical depth, as shown in the fourth and fifth columns of Table 2.1. Again, our result for WMAP3 is consistent with the result from the WMAP collaboration, although, different from the WMAP collaboration, we do not include the BB spectrum in the analysis of the three-year data. The first year results are consistent with the three-year results despite a relatively high matter density.

Table 2.2 lists our best fit non-running models when using different data sets. The first column is the result from the first year WMAP data alone (same as the second column of Table 2.1); others are from the combinations of the first year WMAP data and the data sets specified in the first row, where CMB = ACBAR + CBI + VSA is the combination of the recent CMB data [18, 19, 20] and LSS = 2dF + SDSS is the up-

[3]We used most default settings in CosmoMC.

to-date large-scale structure data [21, 22]. We used the July 2005 version of CosmoMC and its default data sets in the analysis including the first year WMAP data. These data sets are: July 2002 ACBAR data [18], $900 \leq l \leq 1950$ (7 data points); 2000 and 2001 CBI data [19], $700 \leq l \leq 1760$ (8 data points); February 2004 VSA data [20], $640 \leq l \leq 1700$ (8 data points); June 2002 2dF data [21], $0.022 \leq k(h/\mathrm{Mpc}) \leq 0.147$, 32 data points; October 2003 SDSS data [22], $0.016 \leq k(h/\mathrm{Mpc}) \leq 0.205$ (19 data points). These data are combined in the standard way: For WMAP data, CosmoMC uses the WMAP likelihood function; for other data, the code is usually fed into CosmoMC by the corresponding experimental group.[4]

Table 2.2: Best fit non-running models for the combinations of the first year WMAP and other data sets.

Parameter	WMAP1a	CMB	2dF	CMB+2dF	SDSS	LSS	All
n_s	0.96	0.96	0.97	0.96	0.99	0.99	0.96
A	0.87	0.86	0.87	0.86	0.90	0.90	0.86
τ	0.11	0.12	0.11	0.11	0.13	0.15	0.091
h	0.69	0.71	0.69	0.70	0.67	0.69	0.68
$100\Omega_b h^2$	2.29	2.28	2.29	2.29	2.38	2.37	2.29
$\Omega_m h^2$	0.145	0.136	0.145	0.140	0.160	0.152	0.149
100θ	1.045	1.043	1.045	1.044	1.050	1.049	1.045
χ^2	1428.8	1449.3	1463.2	1484.3	1453.5	1490.0	1513.0
ν	1342	1365	1374	1397	1361	1393	1416

Table 2.3 lists similar best fit non-running models as Table 2.2, with the first

[4]We found a bug in the CBI data set. The offset lognormal matrix for CBI is inconsistent with its data. See Ref. [23] for a discussion about the impact of using the wrong matrix; also see the CBI website, http://www.astro.caltech.edu/~tjp/CBI/data, for a link to the discussion about this issue. Since this bug was found after the initial submission of this thesis, the corresponding best fit models in Tables 2.2, 2.3, 2.5, and 2.6, are recollected using the right matrix. The modifications to the initial submission, however, are not significant: The best fit models are basically unchanged and the χ^2's are down-shifted by 3.1 to 3.8.

year WMAP data replaced by the three-year data. We used the May 2006 version of CosmoMC in the analysis including the three-year WMAP data.[5] Except for using the 2005 2dF data (the same range of k/h and the same number of data points as 2002 2dF data) [24], other data sets are the same as those in Table 2.2.[6] Tables 2.2 and 2.3 show that including other data sets has only minor effects on the parameters, while the large-scale structure data favor a slightly larger matter density.

Table 2.3: Best fit non-running models for the combinations of the three-year WMAP and other data sets.

Parameter	WMAP3a	CMB	2dF	CMB+2dF	SDSS	LSS	All
n_s	0.95	0.95	0.95	0.95	0.95	0.96	0.95
A	0.81	0.80	0.80	0.80	0.84	0.82	0.83
τ	0.090	0.088	0.085	0.080	0.071	0.082	0.074
h	0.73	0.73	0.73	0.72	0.66	0.69	0.69
$100\Omega_b h^2$	2.22	2.20	2.22	2.20	2.24	2.26	2.22
$\Omega_m h^2$	0.128	0.125	0.127	0.127	0.146	0.141	0.138
100θ	1.040	1.039	1.039	1.039	1.041	1.042	1.040
χ^2	11252.3	11271.5	11290.9	11310.2	11285.1	11327.0	11348.1

Figure 2.1 shows the distributions of the parameters for the non-running model using the three-year WMAP data, where solid lines are marginalized probabilities and dotted lines are mean likelihoods of samples; for Gaussian distributions they should be the same.[7] There are four independent Markov chains, each having 200,000 samples. After removing burn-in samples, there are about 8×10^4 accepted samples from which

[5]Column WMAP3a of Tables 2.1 and 2.3 is obtained from the April 2006 CosmoMC, but there should be no difference between the April and May 2006 CosmoMC at this level.

[6]We used the default settings for the data sets in CosmoMC. The SDSS likelihood is computed from $k/h = 3.16 \times 10^{-3}$ to 1Mpc^{-1} in the July 2005 CosmoMC, but from $k/h = 10^{-4}$ to 1Mpc^{-1} in the May 2006 CosmoMC; however, the difference seems negligible.

[7]See http://www.cosmologist.info/cosmomc.

the distributions are generated. As shown in the figure, the chains converge very well.

To summarize this section, the non-running model with a nearly scale-invariant spectrum fits the WMAP data and other up-to-date CMB and large-scale structure data very well.

2.2 Large Running Power Spectrum

Although a nearly scale-invariant spectrum fits the data very well, a running power spectrum is also consistent with the current data. In 2003 the first year WMAP data opened the door to the possibility of a large running power spectrum $\alpha_s = -0.1$, from blue ($n_s > 1$) to red ($n_s < 1$), as shown in Figure 2.2. The -0.1 level of running is uncomfortably large for slow-roll inflation, since the running is a second order effect in the slow-roll expansion; thus it is expected to be small. Therefore, despite the large error bars for the running, it gives rise to a challenge to slow-roll inflation. We discuss the experimental evidence for the running in this section and the theoretical aspects in Chapter 6.

It is obvious that using extra degrees of freedom, the goodness of fit will improve. To quantify the improvement of the goodness of fit, we define

$$\Delta\chi^2 = \chi^2(\text{non-running}) - \chi^2(\text{running}). \tag{2.4}$$

We found that a large tensor contribution is important for obtaining significant improvement. If the tensor-to-scalar ratio is set to $r = 0$, then $\Delta\chi^2 = 1$; however, including the tensor-to-scalar ratio as a free parameter it becomes $\Delta\chi^2 = 5$.[8] We refer to the running spectral index model with tensor spectrum as the running model.[9]

[8]Note that the improvement is $\Delta\chi^2 = 3$ in the WMAP best fit model [11, 12]. Moreover, the improvement is $\Delta\chi^2 = 3$ for the three-year WMAP data whether tensor spectrum is included or not [13]. See Table 2.4 for comparison.

[9]To be consistent with the WMAP collaboration, the tensor spectral index is given by the inflationary consistency equation, $n_t = -r/8$, which is a good approximation at this level of running. See Section 6.2 for a more rigorous treatment for the tensor spectrum.

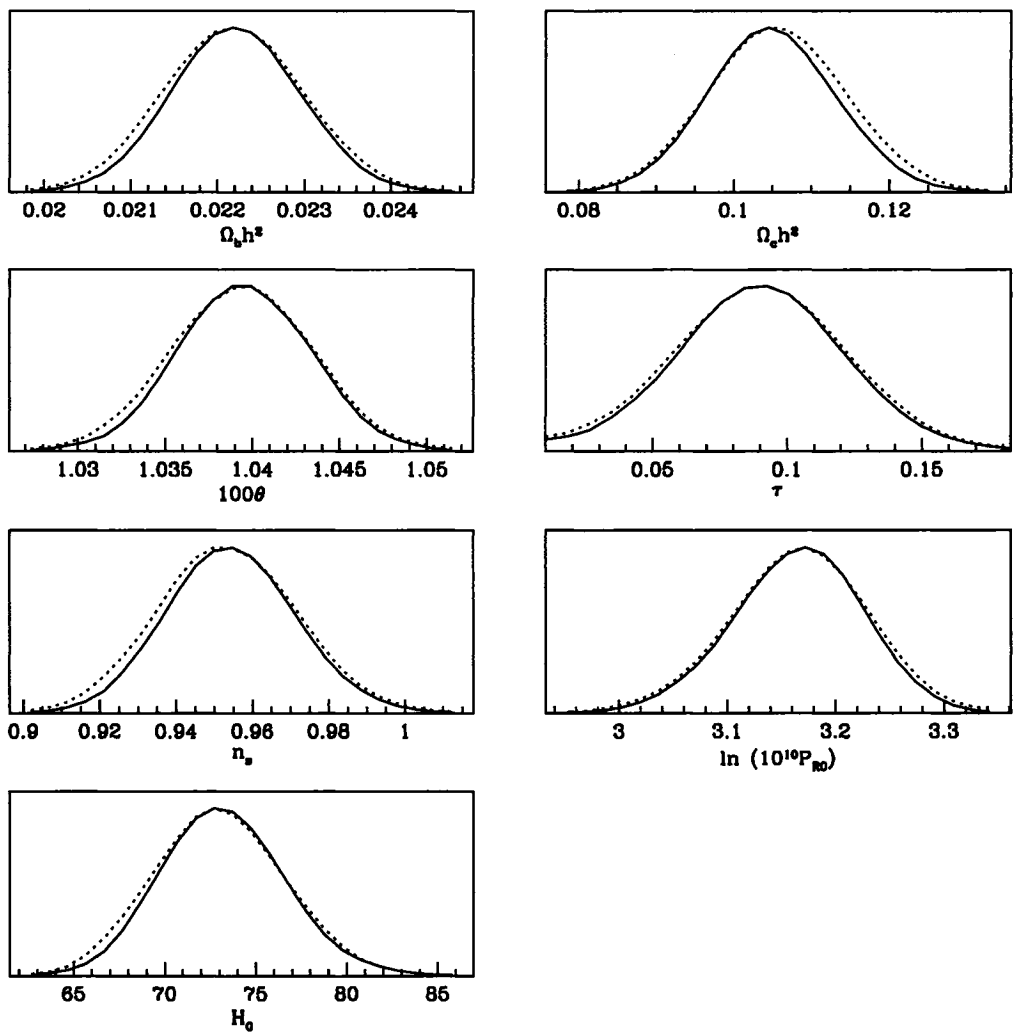

Figure 2.1: The parameter distributions for the non-running model using the three-year WMAP data. Solid lines are marginalized probabilities and dotted lines are mean likelihoods of samples.

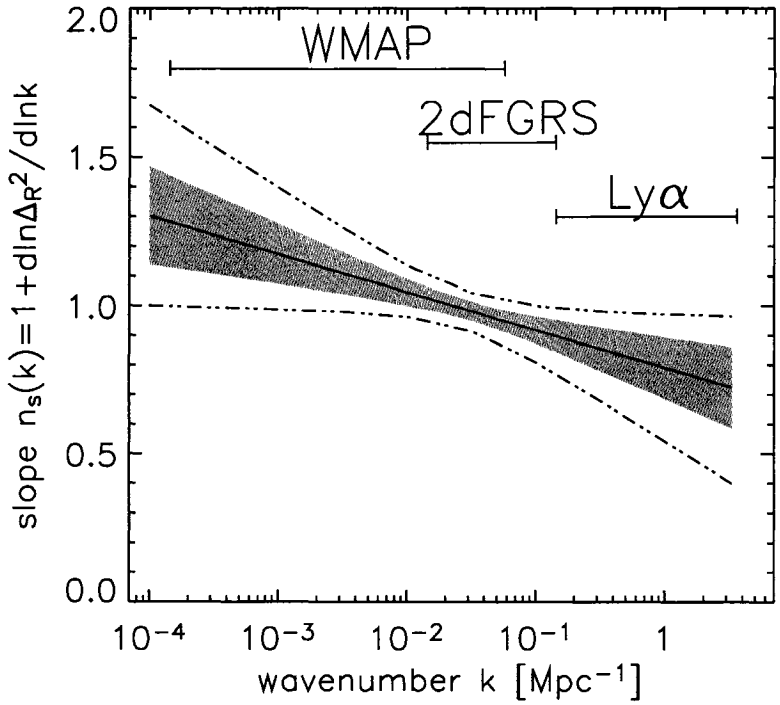

Figure 2.2: The spectral index n_s as a function of k for the combination of the first year WMAP and other data. The mean (solid line), the 68% (shaded area), and the 95% (dashed lines) intervals are shown. The scales probed by the data are indicated on the figure. (Reproduced from Figure 2 of Ref. [12].)

Table 2.4 lists the best fit running models for the first year and three-year WMAP data. With the improvement of measurements of the three-year data, the level of running is still large, but it is reduced in our best fit model of the three-year data. It can be seen that there is a large discrepancy between columns WMAP3 and WMAP3b in Table 2.4. First of all, Ref. [13] does not provide the best fit running model, and the values listed in column WMAP3 of Table 2.4 are marginalized values. Moreover, the Sunyaev-Zel'dovich effect is considered in Ref. [13], but it is not considered in our analysis. Actually, including this secondary effect seems to have little effect on the best fit model. Finally, the constraints on the parameters have been narrowed by new chains run by the WMAP collaboration since the first release of the WMAP3 paper [13]. The up-to-date results are available on the WMAP website,[10] and the

[10]See http://lambda.gsfc.nasa.gov/product/map/dr2/parameters.cfm.

new marginalized values for the running model are $n_s = 1.16$, $\alpha_s = -0.085$, and $r < 1.1$ (95% CL). Therefore, the new result confirms the trend of shrinking the level of running and the tensor-to-scalar ratio, as has been pointed out by our best fit running model for the three-year WMAP data.[11]

Figure 2.3 shows the distributions of the parameters for the running model using the three-year WMAP data. There are four Markov chains, each having 200,000 samples. After removing burn-in samples, there are about 3×10^4 accepted samples from which the distributions are generated. These chains, however, do not converge as well as those of the non-running model.

Tables 2.5 and 2.6 list our best fit running models for the combinations of the first year and three-year WMAP and other data sets. It can be seen that including other CMB data the $\Delta\chi^2$'s go from 4.8 to 7.3 and from 3.1 to 3.9 for first year and three-year WMAP data respectively, so the CMB data strengthen the evidence for running (other parameters remain basically unchanged). Meanwhile, inclusion of large-scale structure data reduces both the $\Delta\chi^2$'s and the values of n_s, α_s, and the tensor-to-scalar ratio r.[12] So large-scale structure data do not favor running. From the first to three-year WMAP data (and their combinations), the spectral index and the tensor-to-scalar ratio are reduced, especially for the tensor-to-scalar ratio when

[11]For the three-year data, we found a best fit point with $\Delta\chi^2 = 648$, which is a huge change of χ^2, and this model is very different from those given in Table 2.4, notably with a positive running spectral index, $\alpha_s = 0.07$. With detailed investigation, we found that the decrease of χ^2 mainly comes from the fact that the TT beam and point source correction (see Ref. [9]) is almost identical to the TT high multipole χ^2, 114374, but with the opposite sign and hence the total χ^2 is reduced significantly. We suspect the validity of the beam and point source corrections code released by the WMAP collaboration, `WMAP_3yr_tt_beam_and_ptsrc_corr.f90`, in the range of a positive running spectral index, and we do not regard this point as a real best fit. The author of the code, Michael Nolta, informed us that this may be due to the failure of the gaussian approximation of the likelihood (private communication).

[12]In trying to understand why the SDSS analysis [22] favors running, but our best fit running model using SDSS data does not, we note that the SDSS analysis uses a non-flat model when running is considered.

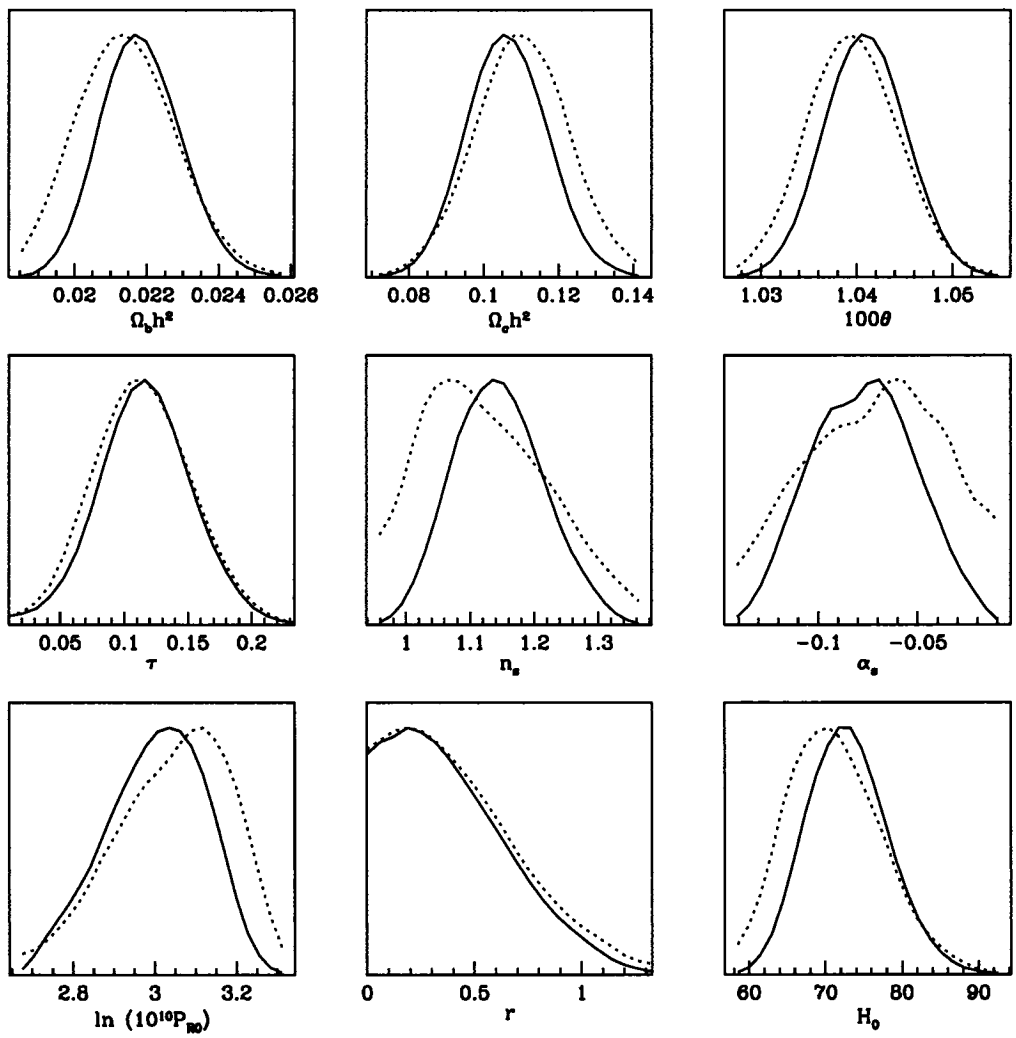

Figure 2.3: The parameter distributions for the running model using the three-year WMAP data. Solid lines are marginalized probabilities and dotted lines are mean likelihoods of samples.

Table 2.4: Best fit running models for the first year and three-year WMAP data.

Parameter	WMAP1 [12]	WMAP1c	WMAP3[a] [13]	WMAP3b
n_s	1.27	1.27	1.21	1.12
α_s	-0.10	-0.098	-0.10	-0.076
r	0.56	0.57	< 1.5 (95% CL)	0.24
A	0.74	0.72	0.61[b]	0.74
τ	0.29	0.29	0.11	0.12
h	0.79	0.81	0.74	0.70
$100\Omega_b h^2$	2.3	2.39	2.20	2.13
$\Omega_m h^2$	0.122	0.122	0.126	0.132
100θ	–	1.050	–	1.039
$\Delta\chi^2$	3	4.8	3	3.1

[a]Ref. [13] does not give the best fit running model; here we list the marginalized (mean) values. Besides, the Sunyaev-Zel'dovich effect is considered here.

[b]The original value is $\mathcal{P}_{\mathcal{R}0}(0.05) = 20.9 \times 10^{-10}$. Here we take $n_s = 1.21$ and $\alpha_s = -0.102$ to evaluate $A(0.002)$.

the SDSS data is included.

The fact that CMB data favor running, but large-scale structure data do not, implies that the evidence of running actually comes from the low-k part of the power spectrum, where the CMB is more sensitive. This suggests that the real power spectrum may be more complicated than the parameterization as Eq. (2.2). We were therefore motivated to introduce the partial running model, which has a running spectrum in the relevant part of the k space but is flat in low and high k regions [25]. We tuned the range of running to be as small as possible until the χ^2 increases. For the first year and three-year WMAP data, the relevant ranges for running are $-7.2 < \ln k\ [\mathrm{Mpc}^{-1}] < -2.8$ and $-6.6 < \ln k\ [\mathrm{Mpc}^{-1}] < -2.8$ respectively. Regions of running for other data sets are given in the lower parts of Tables 2.5 and 2.6. Figures 2.4 and 2.5 show the corresponding best fit non-running, running, and the

Table 2.5: Best fit running models for the combinations of the first year WMAP and other data sets.

Parameter	WMAP1c	CMB	2dF	CMB+2dF	SDSS	LSS	All
n_s	1.27	1.27	1.09	1.09	1.09	1.09	1.09
α_s	−0.098	−0.098	−0.047	−0.051	−0.040	−0.036	−0.045
r	0.57	0.57	0.24	0.23	0.24	0.24	0.23
A	0.72	0.72	0.79	0.79	0.79	0.79	0.79
τ	0.29	0.29	0.14	0.13	0.14	0.14	0.13
h	0.81	0.81	0.69	0.69	0.68	0.68	0.68
$100\Omega_b h^2$	2.39	2.40	2.28	2.26	2.34	2.38	2.32
$\Omega_m h^2$	0.122	0.122	0.146	0.144	0.152	0.155	0.149
100θ	1.050	1.050	1.046	1.046	1.046	1.050	1.046
$\Delta\chi^2$	4.8	7.3	1.4	2.6	−2.4	0.2	−0.4
$\ln k_{\rm low}$	−7.2	−7.5	−6.4	−6.5	−6.5	−6.5	−6.5
$\ln k_{\rm high}$	−2.8	−2.3	−2.6	−2.5	−2.8	−2.7	−2.6
$\Delta\chi^2$	4.7	7.4	1.9	2.9	−0.1	1.7	2.2

corresponding partial running models for WMAP. Since other CMB data strengthen the evidence for running, but large-scale structure data weaken it, when including large-scale structure data, the lower cutoff will be larger than, and the higher cutoff will be smaller than, those including other CMB data. This effect, however, is not obvious for the three-year WMAP data since its evidence for running is weaker than that of the first year data. Except for WMAP1c and WMAP1c+SDSS, other χ^2 values for the partial running model are seen to be lower than those of the running and non-running models.

It is at first surprising that the running region of the spectrum can be reduced to such an extent. Moreover, Ref. [26] claimed that the evidence for running mainly comes from the lowest three multipoles. This is in contrast to the running part of our partial running spectrum since roughly speaking, $k/a_0H_0 \sim l/2$, and hence the

Table 2.6: Best fit running models for the combinations of the three-year WMAP and other data sets.

Parameter	WMAP3b	CMB	2dF	CMB+2dF	SDSS	LSS	All
n_s	1.12	1.11	1.06	1.16	1.05	1.03	1.05
α_s	−0.076	−0.073	−0.049	−0.086	−0.046	−0.034	−0.048
r	0.24	0.13	0.12	0.33	0.0023	0.034	0.0069
A	0.74	0.76	0.76	0.70	0.84	0.82	0.82
τ	0.12	0.12	0.10	0.12	0.10	0.10	0.086
h	0.70	0.70	0.70	0.71	0.63	0.67	0.65
$100\Omega_b h^2$	2.13	2.11	2.14	2.15	2.17	2.20	2.14
$\Omega_m h^2$	0.132	0.132	0.130	0.131	0.153	0.144	0.147
θ	1.039	1.040	1.038	1.040	1.041	1.041	1.041
$\Delta\chi^2$	3.1	3.9	2.7	3.2	3.2	0.5	1.4
$\ln k_{\rm low}$	−6.6	−6.5	−6.5	−6.5	−6.4	−6.5	−6.5
$\ln k_{\rm high}$	−2.8	−2.3	−2.6	−2.6	−2.6	−2.7	−2.4
$\Delta\chi^2$	3.7	4.9	3.1	4.6	6.0	4.0	4.5

lower cutoff $\ln k_{\rm low} = -7.2$ corresponds to $l \sim 6$. To better understand this, we have computed the difference in χ^2 between the best fit non-running and running models including contributions from $l_{\rm min}$ to $l_{\rm max}$:[13]

$$\Delta\chi^2(l_{\rm min}) = \sum_{l=l_{\rm min}}^{l_{\rm max}} \delta\chi^2(\text{non-running}) - \delta\chi^2(\text{running}), \tag{2.5}$$

where $\delta\chi^2(l)$ is the χ^2 contributed from diagonal (l) and off-diagonal ($l' > l$) terms. For the three-year WMAP data, TT beam and point source corrections and TE determinant likelihoods are also included.[14] The plots are shown in Figures 2.6, and 2.7. We observe there that the low multipoles ($l = 2, 3, 4$) in the TT data do account

[13] $l_{\rm max} = 900$ for the first year WMAP TT spectrum, 1000 for the three-year WMAP TT spectrum, and 450 for the TE spectra.

[14] There is a bug in the code, `WMAP_3yr_tt_beam_and_ptsrc_corr.f90`, provided by the WMAP collaboration, where the C_l spectra are incorrectly passed into the function

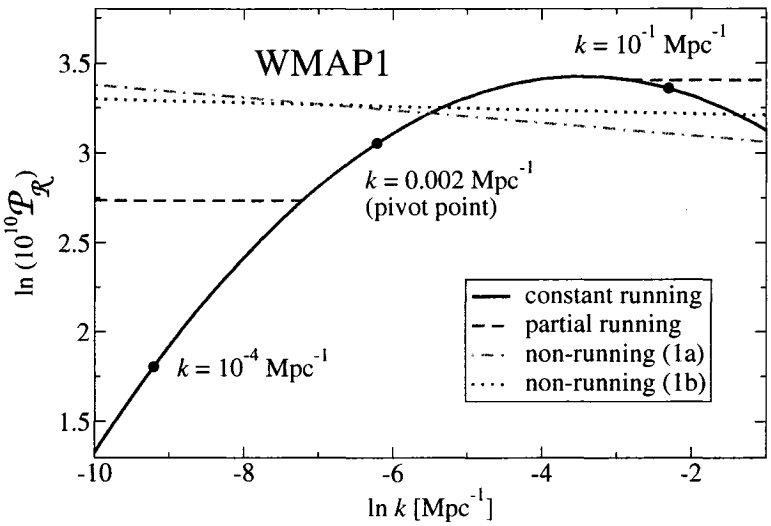

Figure 2.4: The best fit power spectra of the first year WMAP data: constant running (solid, black), partial running (dashed, red), and non-running (1a: dot-dashed, green; 1b: dotted, blue).

for cumulative contributions to the total decrease in χ^2 between the non-running and running models ($\Delta\chi^2_{\rm TT} = 0.5$ and 1.0 for WMAP1ac and WMAP1bc respectively). However the TE data, ignored by the analysis of Ref. [26], have the opposite effect and hence the $\Delta\chi^2_{\rm tot}$ is rather insensitive to the inclusion of the first three multipoles. In fact, the larger part of the decrease in χ^2 clearly comes from the regions near $l = 7$ in the TE data ($\Delta\chi^2_{\rm TE} = 1.7$ for both WMAP1ac and WMAP1bc) and $l = 40$ in the TT data (from $l = 37$ to 44, $\Delta\chi^2_{\rm TT} = 1.2$, 2.3, and 2.2 for WMAP1ac, WMAP1bc, and WMAP3ab respectively). Again, the decrease of χ^2 in $l = 7$ is compensated by opposite effect of the low multipoles in the TE data. Nevertheless, the multipoles near $l = 40$ explain why our partial running spectrum starts running at relatively high k values, $k \sim 0.001$ Mpc^{-1}, compared to the the values which would affect the low multipoles, $k \sim 10^{-4}$ Mpc^{-1}. This perspective lends more interest to the possible confirmation or negation of large running by future improvements in the data, since the experimental determination of the higher multipoles is not so limited by cosmic

---

`compute_tt_beam_and_ptsrc_chisq` due to the range of dynamical allocation of the storage space of the C_l arrays. We have avoided this problem and reported this bug to the author of the code.

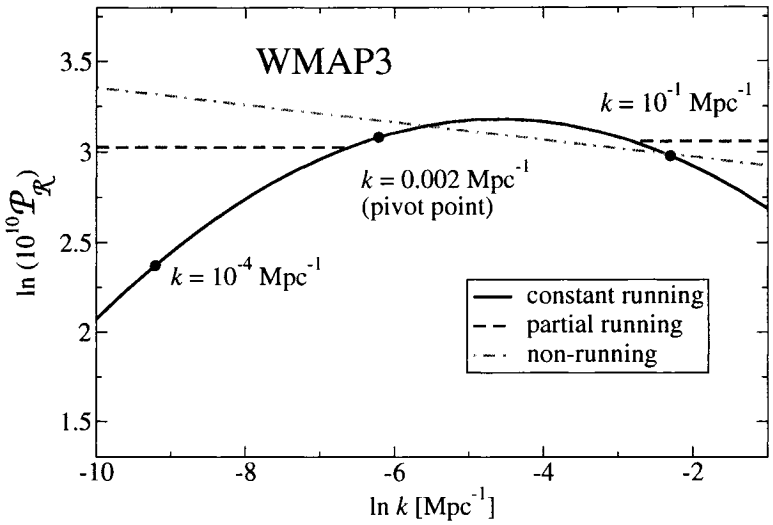

Figure 2.5: The best fit power spectra of the three-year WMAP data: constant running (solid, black), partial running (dashed, red), and non-running (dot-dashed, green).

variance [25].

To summarize this section, we found that the evidence for running mainly comes from multipoles near $l = 40$, and hence a partial running model with a small region of running would give as good a fitting as the full running model. Although the goodness of fit, $\Delta\chi^2 = 3$, does not justify adding two extra parameters, the possibility of a large running power spectrum is still interesting since it is unexpected in slow-roll inflation.

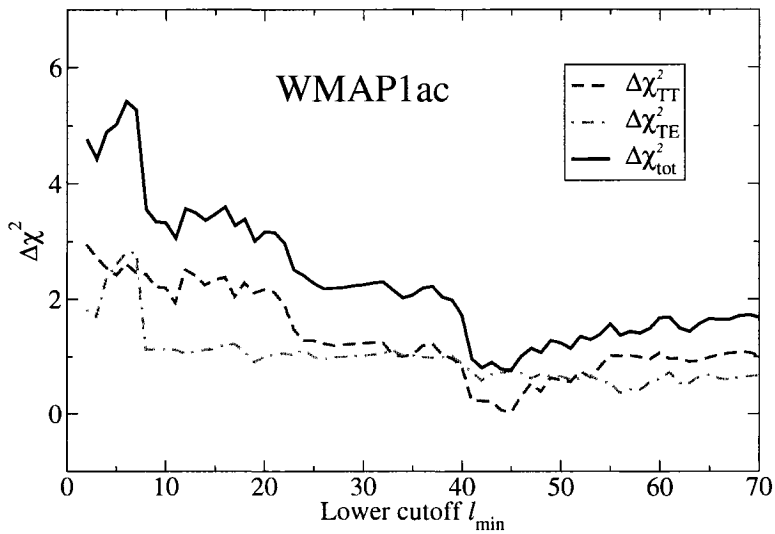

(a)

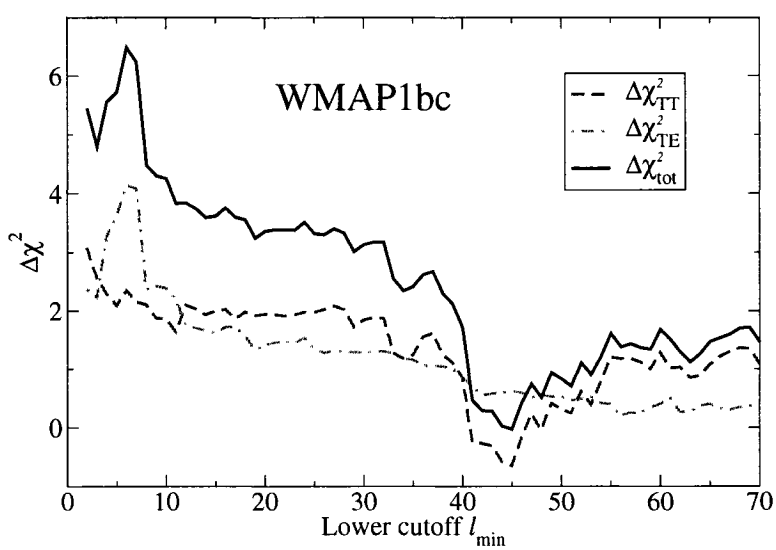

(b)

Figure 2.6: Difference of χ^2 between the best fit non-running and running models of the first year WMAP data (a: 1a and 1c; b: 1b and 1c), versus the minimum multipole included $l_{\rm min}$. The separate contributions from temperature (TT) and polarization (TE) as well as the total are shown.

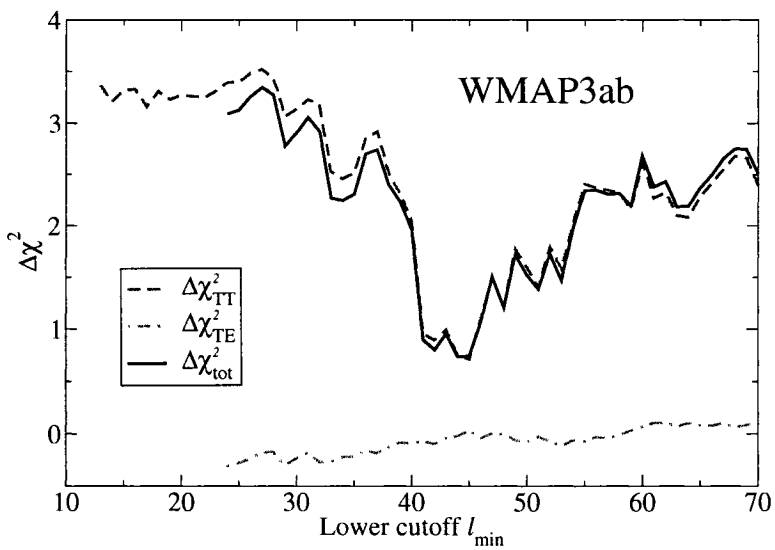

Figure 2.7: Difference of χ^2 between the best fit non-running and running models of the three-year WMAP data (3a and 3b), versus the minimum multipole included $l_{\rm min}$. The separate contributions from temperature (TT) and polarization (TE) as well as the total are shown.

Chapter 3

Inflationary Spectral Index

There has been interest in the accuracy of the slow-roll approximation since it was presented. Higher order corrections in the power spectrum and the spectral indices have been calculated [27, 28]. New approximate methods have also been invented to better describe the inflationary dynamics, *e.g.* the inflation flow equations [29, 30], the horizon-flow slow-roll parameters [31, 32], and the uniform approximation [33]; see Ref. [34] for a recent review. In this chapter, we present formulae for spectral indices and their runnings based on the Hamilton-Jacobi formulation of inflation, which allows for a rigorous treatment of the inflaton equation of motion. In addition, these formulae are also useful in potential reconstruction, as will be illustrated in Chapters 5 and 6.

3.1 Hamilton-Jacobi Formulation of Inflation

The basic idea of the Hamilton-Jacobi formulation of inflation is to regard the Hubble parameter $H(\phi)$, rather than the inflaton potential $V(\phi)$, as the fundamental quantity [35, 36], which can reduce the second order differential equation to a first order equation. Differentiating Eq. (1.10) with respect to time and substituting into Eq. (1.11) gives

$$\dot{\phi}^2 = -2\dot{H}. \tag{3.1}$$

Assuming ϕ is a strictly monotonic function of time during inflation (if that is not the case, we can focus on monotonic epochs and patch them together), so $\dot{\phi} \neq 0$ and the inflaton field can be regarded as the basic variable during inflation. Dividing Eq. (3.1) by $\dot{\phi}$ and substituting into Eq. (1.10), one has

$$\dot{\phi} = -2H', \tag{3.2}$$

$$V = 3H^2 - 2H'^2. \tag{3.3}$$

These equations look like those of the Hamilton-Jacobi formalism in classical mechanics, and Eq. (3.3) is referred to as the Hamilton-Jacobi equation [36].

The Hamilton-Jacobi formulation of inflation provides an easy way to find exact solutions. Once the Hubble parameter is specified, the potential as well as the scalar field can be obtained exactly (if Eq. (3.2) can be integrated analytically). Moreover, this rigorous treatment of the equation of motion does not depend on the inflationary attractor behavior, which is crucial to the validity of the potential slow-roll approximation; see the discussion in Section 4.3.

Like the potential slow-roll parameters, the Hubble slow-roll parameters are defined as [27, 15]

$$\epsilon_{\rm H} = 2\left(\frac{H'}{H}\right)^2, \tag{3.4}$$

$$\eta_{\rm H} = 2\frac{H''}{H}, \tag{3.5}$$

$$\xi_{\rm H} = 4\frac{H'}{H}\frac{H'''}{H}. \tag{3.6}$$

Using the Hamilton-Jacobi equation, the potential slow-roll parameters can be expressed in terms of the Hubble slow-roll parameters exactly [15]. In first order of the slow-roll approximation, their relations are

$$\epsilon_{\rm H} \simeq \epsilon_{\rm V}, \tag{3.7}$$

$$\eta_{\rm H} \simeq \eta_{\rm V} - \epsilon_{\rm V}, \tag{3.8}$$

$$\xi_{\rm H} \simeq \xi_{\rm V} - 3\epsilon_{\rm V}\eta_{\rm V} + 3\epsilon_{\rm V}^2. \tag{3.9}$$

We use the Hubble slow-roll parameters and drop the subscript H hereafter unless there is an ambiguity.

Using the slow-roll parameter ϵ, the Einstein field equation, Eq. (1.3), can be written as

$$\frac{\ddot{a}}{a} = (1-\epsilon)H^2. \tag{3.10}$$

Therefore, $\ddot{a} > 0 \Longleftrightarrow \epsilon < 1$ and the end of inflation is indicated by $\epsilon = 1$ exactly. As for the number of e-foldings, it can be written as

$$N = \frac{1}{2}\int_{\phi_{\rm end}}^{\phi} \frac{H}{H'} d\phi, \tag{3.11}$$

which gives two useful relations:

$$\frac{dN}{d\phi} = \frac{1}{2}\frac{H}{H'} \qquad \text{and} \qquad \frac{d\phi}{dN} = 2\frac{H'}{H}. \tag{3.12}$$

The derivatives of the slow-roll parameters with respect to N follow directly [29]:

$$\frac{d\epsilon}{dN} = 2\epsilon(\eta - \epsilon), \tag{3.13}$$

$$\frac{d\eta}{dN} = \xi - \epsilon\eta, \tag{3.14}$$

$$\frac{d\xi}{dN} = (\eta - 2\epsilon)\xi + \sigma, \tag{3.15}$$

where σ is another slow-roll parameter [15]:

$$\sigma = 8\frac{H'^2 H''''}{H^3}. \tag{3.16}$$

3.2 Inflationary Spectral Indices

Differentiating the horizon crossing condition, one has the relation between the number of e-foldings and the comoving wavelength:

$$\frac{dN}{d\ln k} = \frac{-1}{1-\epsilon}. \tag{3.17}$$

From the power spectra of the primordial curvature perturbation and gravitational waves, Eqs. (1.21) and (1.22), and the derivatives of the slow-roll parameters, Eqs. (3.13) and (3.14), the spectral indices and their running follow straightforwardly:

$$n_s - 1 = \frac{2}{1-\epsilon}(\eta - 2\epsilon), \tag{3.18}$$

$$n_t = \frac{-2\epsilon}{1-\epsilon}, \tag{3.19}$$

$$\alpha_s = \frac{-2}{(1-\epsilon)^3}[4\epsilon^2 - 5\epsilon\eta + \xi + \epsilon(-\epsilon\eta + 2\eta^2 - \xi)], \tag{3.20}$$

$$\alpha_t = \frac{-4\epsilon}{(1-\epsilon)^3}(\epsilon - \eta). \tag{3.21}$$

Dropping the ϵ terms in the denominators and $O(\epsilon^3)$ order terms in α_s, one recovers the standard results at first order in the slow-roll approximation; see Eqs. (1.30), (1.31), (1.34), and (1.35). In slow-roll inflation, the Hubble parameter is basically unchanged so the ϵ terms in the denominators are negligible; nevertheless, we will see that the ϵ term in the horizon crossing condition improves the accuracy and plays an important role in potential reconstruction.

In terms of the Hubble slow-roll parameters, the tensor-to-scalar ratio is

$$r(k) = 16\epsilon(k), \tag{3.22}$$

which gives the inflationary consistency equation:

$$n_t = -\frac{1}{1-r/16}\frac{r}{8} < -\frac{r}{8}. \tag{3.23}$$

It is an inequality rather than an equality as the potential slow-roll approximation predicts. Also note that α_t is a function of ϵ and η, which can be expressed as a combination of n_s and n_t:

$$\alpha_t = n_t[n_t - (n_s - 1)]\left(\frac{2-n_t}{2}\right). \tag{3.24}$$

Differentiating the consistency equation also gives this result, which is known as the second consistency equation [37] (the last parenthesis is the correction from keeping ϵ terms in the denominators).

3.3 Corrections to the Spectral Indices

Eqs. (1.21) and (1.22) are the standard results to first order in the slow-roll approximation; the second order results are [27]

$$\mathcal{P}_{\mathcal{R}}^{(2)}(k) = [1 - \epsilon + (2 - \ln 2 - \gamma)(2\epsilon - \eta)]^2 \left(\frac{H^2}{2\pi\dot{\phi}}\right)^2\Bigg|_{k=aH}, \tag{3.25}$$

$$\mathcal{P}_h^{(2)}(k) = 8\left[1-(\ln 2-1+\gamma)\epsilon\right]^2\left(\frac{H}{2\pi}\right)^2\Bigg|_{k=aH}, \tag{3.26}$$

where $\gamma \simeq 0.5772$ is the Euler-Mascheroni constant. The corresponding spectral indices are [27, 15]

$$n_s^{(2)}-1 = -4\epsilon+2\eta-2(1+c)\epsilon^2-\frac{1}{2}(3-5c)\epsilon\eta+\frac{1}{2}(3-c)\xi, \tag{3.27}$$

$$n_t^{(2)} = -2\epsilon-(3+c)\epsilon^2+(1+c)\epsilon\eta, \tag{3.28}$$

where $c = 4(\ln 2+\gamma)-5 \simeq 0.08145$. From the derivatives of the slow-roll parameters, Eqs. (3.13) to (3.15), here we present the runnings of spectral indices to $O(\epsilon^3)$ order (for α_s) in the slow-roll approximation:

$$\begin{aligned}\alpha_s^{(2)} &= \frac{-1}{1-\epsilon}\Big[8\epsilon^2-10\epsilon\eta+2\xi+8(1+c)\epsilon^3-\frac{1}{2}(7+31c)\epsilon^2\eta \\ &\quad -(3-5c)\epsilon\eta^2-\frac{1}{2}(9-7c)\epsilon\xi+\frac{1}{2}(3-c)\eta\xi+\frac{1}{2}(3-c)\sigma\Big],\end{aligned} \tag{3.29}$$

$$\begin{aligned}\alpha_t^{(2)} &= \frac{-\epsilon}{1-\epsilon}\Big[4\epsilon-4\eta+4(3+c)\epsilon^2-(15+7c)\epsilon\eta+(1+c)\xi \\ &\quad +2(1+c)\eta^2\Big].\end{aligned} \tag{3.30}$$

It is obvious that the second order results agree with the potential slow-roll approximation to first order; see Eqs. (1.30), (1.31), (1.34), and (1.35).

The exact results to first order, Eqs. (3.18)-(3.21), may not be as good as the approximate results to second order or the methods in Refs. [27, 28, 29, 30, 31, 32, 33] in general; nevertheless, these simple formulae, which are the results of keeping the ϵ term in the horizon crossing condition, are still theoretically interesting. First of all, there are two exact solutions to the original perturbation equations, power-law inflation [27] and the $n_s = 3$ case [38]. The perturbation equations are [27]

$$\frac{d^2u_k}{d\tau^2}+\left(k^2-\frac{1}{z}\frac{d^2z}{d\tau^2}\right)u_k = 0, \tag{3.31}$$

$$\frac{d^2v_k}{d\tau^2}+\left(k^2-\frac{1}{a}\frac{d^2a}{d\tau^2}\right)v_k = 0, \tag{3.32}$$

with boundary conditions

$$u_k \to \frac{1}{\sqrt{2k}}e^{-ik\tau}, \quad v_k \to \frac{1}{\sqrt{2k}}e^{-ik\tau}, \qquad \text{for } aH \ll k, \tag{3.33}$$

$$u_k \propto z, \qquad v_k \propto a, \qquad \text{for } aH \gg k, \tag{3.34}$$

where $\tau = \int a^{-1}dt$ is the conformal time and $z = a\dot{\phi}/H$; u_k and v_k are the Fourier modes of the scalar perturbation, u, and the tensor perturbation, v, respectively. (See Ref. [27] for details about these quantities.)

In the case of power-law inflation, our simple formulae give the exact spectral indices and the tensor-to-scalar ratio as well (see Section 6.2); although the second order results still give constant spectral indices, they do not predict the right values. In the case of $n_s = 3$, Eq. (3.18) gives the correct result again, but the second order result, Eq. (3.27), gives a running index instead of a constant index [38].[1] Second of all, the ϵ term in the horizon crossing condition is crucial to the accuracy of the reconstruction of inflaton potentials, which will be illustrated in Chapter 4.

Ref. [34] showed that if the slow-roll parameters are of order $o(10^{-1})$, then the second order results are not really necessary; also, in the case of large running spectral index, the second order results do not seem to improve the accuracy. Although we mainly consider the first order results, one can straightforwardly incorporate higher-order corrections into the discussion in this thesis. In brief, the simple formulae remain interesting and useful.

[1]We do not yet understand the reason for our method agreeing with the exact results. This is the subject of future investigations.

Chapter 4

Reconstruction of Inflaton Potentials

As the experimental determinations of the inflationary power spectrum become more and more precise, one might want to extract information of the early universe from the spectral index as much as possible. For instance, what is the inflaton potential which gives the best fit inflationary power spectrum? This issue can be solved through the reconstruction of inflaton potentials. The traditional method of inflaton potential reconstruction is to Taylor expand the potential in terms of the slow-roll parameters, which are determined by a given power spectrum [39]; this method, however, is not always reliable [40]. New methods, such as Monte Carlo reconstruction [41] and analytic reconstruction [42], are still not satisfactory in simplicity and accuracy. In this chapter, we present an integration method for potential reconstruction based on the Hamilton-Jacobi formulation of inflation [35, 36], which is not only accurate but also simple.

4.1 Reconstruction Formulation

Our purpose is to construct $H(\phi)$, and hence $V(\phi)$, from a given $\mathcal{P}_{\mathcal{R}}(k)$, which cannot be done directly because the relation of ϕ and k is given implicitly by the horizon crossing condition, $k = aH$. The strategy to avoid this problem is to regard the

inflaton field ϕ as a single-valued function of k, which is guaranteed to be possible by the definition of inflation Eq. (1.7): During inflation, $d\ln k/dt > 0$, together with the assumption $\dot{\phi}(= -2H') \neq 0$, we have $d\ln k/d\phi \neq 0$:

$$\frac{d\ln k}{d\phi} = -\frac{1}{2}\frac{H}{H'} + \frac{H'}{H}, \tag{4.1}$$

and hence the derivative of the Hubble parameter can be written as

$$H' = \frac{dH}{d\ln k}\left(-\frac{1}{2}\frac{H}{H'} + \frac{H'}{H}\right). \tag{4.2}$$

By straightforward manipulation of the equations, one has

$$H'^2 = -\frac{1}{2}H^2\frac{dH}{d\ln k}\left(H - \frac{dH}{d\ln k}\right)^{-1}, \tag{4.3}$$

$$\left(\frac{d\phi}{d\ln k}\right)^2 = -2\frac{d\ln H}{d\ln k}\left(1 - \frac{d\ln H}{d\ln k}\right). \tag{4.4}$$

Substituting Eq. (4.3) into the expression of $\mathcal{P}_\mathcal{R}$, Eq. (1.21), a first order differential equation results:

$$\frac{dH}{d\ln k} = \frac{-H^3}{8\pi^2\mathcal{P}_\mathcal{R} - H^2}, \tag{4.5}$$

and Eq. (4.4) can be written as

$$\frac{d\phi}{d\ln k} = \pm\frac{H\sqrt{16\pi^2\mathcal{P}_\mathcal{R}}}{8\pi^2\mathcal{P}_\mathcal{R} - H^2}. \tag{4.6}$$

Given a power spectrum $\mathcal{P}_\mathcal{R}(k)$, solving Eq. (4.5) gives $H(k)$, and integrating Eq. (4.6) defines $\phi = \phi(\ln k)$. Using the inverse function $\ln k = \ln k(\phi)$, a potential can be reconstructed through the Hamilton-Jacobi equation. Ref. [43] presented a similar integration method, but used the lowest order slow-roll approximation in each step, and hence their method is not as accurate as the Hamilton-Jacobi formulation which we describe.

Although the tensor spectrum is not experimentally well determined today, one can in principle reconstruct inflaton potentials from a tensor spectrum. Since $\mathcal{P}_h \propto H^2$, the reconstruction formulation is:

$$H(k) = \frac{\pi}{\sqrt{2}}\sqrt{\mathcal{P}_h(k)}, \tag{4.7}$$

$$\left(\frac{d\phi}{d\ln k}\right)^2 = -\frac{d\ln\mathcal{P}_h}{d\ln k}\left(1 - \frac{1}{2}\frac{d\ln\mathcal{P}_h}{d\ln k}\right). \tag{4.8}$$

From Eqs. (4.5) and (4.6), we see that an overall factor A^2 in $\mathcal{P}_{\mathcal{R}}(k)$ contributes factors A in H and A^2 in V, but the dynamics of ϕ and $\ln k$ does not change. So we rescale $\mathcal{P}_{\mathcal{R}}$ to absorb the $8\pi^2$ factor for simplicity, $P = 8\pi^2\mathcal{P}_{\mathcal{R}}$. For definiteness, hereafter we take the positive sign of Eq. (4.6); redefining $\phi \to -\phi$ brings us to the other case. We have

$$\frac{dH}{d\ln k} = \frac{-H^3}{P - H^2}, \tag{4.9}$$

$$\frac{d\phi}{d\ln k} = \frac{H\sqrt{2P}}{P - H^2}. \tag{4.10}$$

There is a pole at $P = H^2$ in the above equations, and it divides the phase space of (P, H^2) into two regions. If we start with $P_i > H_i^2$, then $dH/d\ln k < 0$ and H decreases along with $\ln k$. Even though P decreases along with $\ln k$, $P > H^2$ is always satisfied since whenever H^2 approaches P, $dH/d\ln k$ will diverge and thus H^2 will decrease faster than P. Similarly, if we start with $P_i < H_i^2$, then $dH/d\ln k > 0$ but $P < H^2$ remains unchanged. Therefore, no trajectory can cross over the boundary $P = H^2$ if we numerically reconstruct the Hubble parameter, $H(k)$, through Eqs. (4.9) and (4.10).

The above conclusion gives rise to an interesting observation if we express the slow-roll parameter ϵ in terms of P and H^2:

$$\epsilon = \frac{H^2}{P}. \tag{4.11}$$

Recall that $\epsilon = 1$ indicates the end of inflation, so if we start with $P_i < H_i^2$, inflation does not happen; if $P_i > H_i^2$ is given, inflation never comes to an end by itself. In fact, this pole is a result of the assumption that $\epsilon < 1$ (see the context of Eq. (4.1)); therefore, the trajectories remain in either $\epsilon < 1$ or $\epsilon > 1$, and hence it is an intrinsic problem of this reconstruction formulation.

Since H^2 is always smaller than P during inflation, one can usually neglect the H^2 terms in the denominators of Eqs. (4.9) and (4.10) to avoid the pole. Tracing back to the original equations, this is equivalent to neglecting the ϵ term in the horizon crossing condition (see Eqs. (3.17) and (4.1)). Actually, the pole in $H(k)$ does not

necessarily occur in $H(\phi)$. Combining Eqs. (4.9) and (4.10) gives

$$\frac{dH(\phi)}{d\phi} = -\frac{H^2(\phi)}{\sqrt{2P(k)}}. \tag{4.12}$$

There is no pole at all. Eq. (4.12) is actually Eq. (1.21) with $H' < 0$. Since k is related to ϕ implicitly through the horizon crossing condition, Eq. (4.12) cannot be solved analytically in most cases. We will see examples where Eq. (4.12) can be solved directly or the trajectory can cross over the boundary, $P = H^2$, in Section 5.1. Nevertheless, we will show in Chapters 5 and 6 that for a constant spectral index, there is no natural end to inflation; for a running spectral index, since we do not have analytic solutions and must solve the equations numerically, the pole cannot be avoided and again there is no natural end to inflation.

Actually, only about 10 e-foldings of the inflationary power spectrum are observable, and reconstructed potentials are reliable only in the corresponding regions. Therefore, the above problem of the end of inflation can be solved if one simply assumes that the spectral index no longer preserves pure constant or running at some k. Alternatively, other mechanisms, *e.g.* multiple-field inflation, may also arise to make the constant and running spectral index models realistic.

4.2 Corrections to the Reconstruction Formulation

One may worry that the reconstruction formulation may be inaccurate since we consider only the first order result in the slow-roll approximation. However, it is straightforward to incorporate higher order corrections into the formulation using the horizon crossing condition, which implies

$$\frac{d\ln H}{d\ln k} = \frac{-\epsilon}{1-\epsilon}, \tag{4.13}$$

$$\frac{d^2\ln H}{d\ln k^2} = \frac{2\epsilon}{(1-\epsilon)^3}(\eta-\epsilon), \tag{4.14}$$

$$\frac{d^3\ln H}{d\ln k^3} = \frac{-2\epsilon}{(1-\epsilon)^5}\left[4\epsilon^2 - 7\epsilon\eta + 2\eta^2 + 2\epsilon^3 - 5\epsilon^2\eta + 4\epsilon\eta^2 + (1-\epsilon)\xi\right], \tag{4.15}$$

which in turn give

$$\epsilon = -\frac{d\ln H}{d\ln k}\left(1-\frac{d\ln H}{d\ln k}\right)^{-1}, \tag{4.16}$$

$$\eta = \epsilon + \frac{(1-\epsilon)^3}{2\epsilon}\frac{d^2\ln H}{d\ln k^2}, \tag{4.17}$$

$$\xi = -2\epsilon^2 + 3\epsilon\eta - \frac{2}{1-\epsilon}(1+2\epsilon)(\eta-\epsilon)^2 - \frac{(1-\epsilon)^4}{2\epsilon}\frac{d^3\ln H}{d\ln k^3}. \tag{4.18}$$

To incorporate higher order corrections, for instance $O(\epsilon)$ order corrections, we substitute the above equations into Eq. (3.25):

$$\left(\frac{d\ln H}{d\ln k}\right)^3\left(1-\frac{d\ln H}{d\ln k}\right)^3 = -\frac{H^2}{P}\left\{\frac{1}{2}(2-\ln 2-\gamma)\frac{d^2\ln H}{d\ln k^2}+\frac{d\ln H}{d\ln k}\right.$$
$$\left.-[2+(1-\ln 2-\gamma)]\left(\frac{d\ln H}{d\ln k}\right)^2+[1+(1-\ln 2-\gamma)]\left(\frac{d\ln H}{d\ln k}\right)^3\right\}^2. \tag{4.19}$$

Terms in small parentheses are second order corrections; setting them to zero gives the result in Section 4.1.

Although we do not explicitly show the corresponding reconstruction formulation for other higher order corrections, such as $O(\xi)$ [28], it is straightforward to incorporate them as shown above. This yields increasingly higher order differential equations, whose solutions would require more than one initial condition. Instead of doing so, one can incorporate the corrections into the first order result as follows [25]. Define the correction factor C through Eq. (3.25):

$$P^{(2)}(k) \equiv 8\pi^2\mathcal{P}_{\mathcal{R}}^{(2)}(k) = 2C\left(\frac{H^2}{\dot\phi}\right)^2\Bigg|_{k=aH}, \tag{4.20}$$

$$C \equiv [1-\epsilon+(2-\ln 2-\gamma)(2\epsilon-\eta)]^2. \tag{4.21}$$

First, solve the first order equations, Eqs. (4.9) and (4.10), by a given spectrum P, then one has the leading order Hubble parameter H_0 and correction factor C_0. Second, substituting P/C_0 into the first order equations, yields H_1 and the corresponding correction factor C_1, with H_1 satisfying

$$\frac{P}{C_0} = 2\left(\frac{H_1^2}{\dot\phi}\right)^2\Bigg|_{k=aH_1}. \tag{4.22}$$

Repeating the second step with P/C_i, one obtains the ith iteration of the Hubble parameter, H_i, which gives the power spectrum through second order equation:

$$P_i^{(2)} = 2C_i \left(\frac{H_i^2}{\dot{\phi}}\right)^2 \Bigg|_{k=aH_i} = \frac{C_i}{C_{i-1}} P. \tag{4.23}$$

The iterations $\{C_i\}$ are expected to converge to the true correction factor of Eq. (3.25), so $P_i^{(2)}$ is close to P. In brief, we can reconstruct a Hubble parameter, H_i, which gives a power spectrum close to the original spectrum through the second order equation. This procedure works well for small ϵ_i; for large value of ϵ_i, the corrections are not so close to each other in the beginning. Figure 4.1 shows the first and second order reconstructed power spectra for the best fit WMAP running model. The first order result is identical to the input spectrum ($\ln P$), so it is not shown in the figure. For the second order results, we see that after two iterations, the reconstructed spectrum is close to the original spectrum at large k (late-time). The discrepancies in the beginning are due to the discrepancies of corrections $\{C_i\}$, which can be avoided by fine tuning the initial condition $\dot{\phi}_i$, but the late-time values are insensitive to that due to the attractor behavior, as discussed in the next section.

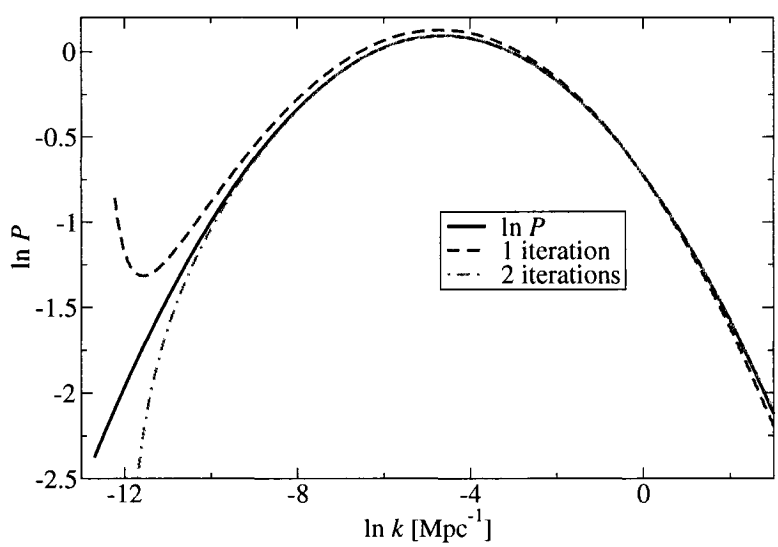

Figure 4.1: The first and second order reconstructed power spectra for the best fit WMAP running model ($n_s = 1.12$, $\alpha_s = -0.076$, $r = 0.24$, and $P_0 = 1$; see column 3b of Table 2.4).

As we have mentioned in Section 3.3, the second order corrections do not necessarily give better results. Therefore, the simple reconstruction formulation remains useful in many cases.

4.3 Inflationary Attractor

Since the original inflationary equation is a second order differential equation, we have, in principle, the freedom to choose the value of $\dot{\phi}_i$ anywhere on the potential; however, in the reconstruction formulation, $\dot{\phi}$ is determined by H', see Eq. (3.2). Figure 4.2 shows the first order reconstructed power spectra for the best fit WMAP running model with different initial inflaton velocities. For $\dot{\phi}_i = -2H'$, the reconstructed spectrum is same as the input power spectrum; for $\dot{\phi}_i \neq -2H'$, there are discrepancies between the shapes of the input and reconstructed spectra. This is because for a given potential, the reconstruction formulation chooses a particular solution of $H(\phi)$, which requires a particular $\dot{\phi}_i$ but gives the desired power spectrum. For example, in the exponential potential case, a complicated, parametric solution $H(\phi)$ is required for arbitrary initial conditions [36], which gives neither power-law expansion nor constant spectral index (see section 5.1). There are also shifts of k for different initial conditions; they come from the definition $\ln k = \ln a + \ln H$ in our algorithm where we choose $a_i = 1$. These shifts, however, do not have absolute meanings since the scale factor is not determined. Also, the normalization factor $8\pi^2\mathcal{P}_{\mathcal{R}0}$ is not included in the numerical calculations; restoring this factor will give a contribution $\sqrt{8\pi^2\mathcal{P}_{\mathcal{R}0}}$ to H, and hence an extra shift of k. Therefore, we shift all reconstructed spectra to the same k_i, the starting point of the input power spectrum. Note that Figure 4.2 is similar to Figure 4.1 except for the shifts (we take $\dot{\phi}_i = -2H'$ in Figure 4.1), and hence the discrepancies of iterations in the beginning can be removed by fine tuning the initial conditions.

The attractor behavior of the Hamilton-Jacobi equation alleviates this initial condition problem [36, 15]. For example, the power-law solution, Eq. (5.3), is the attractor of the exponential potential, Eq. (5.4); all trajectories converge to the attractor

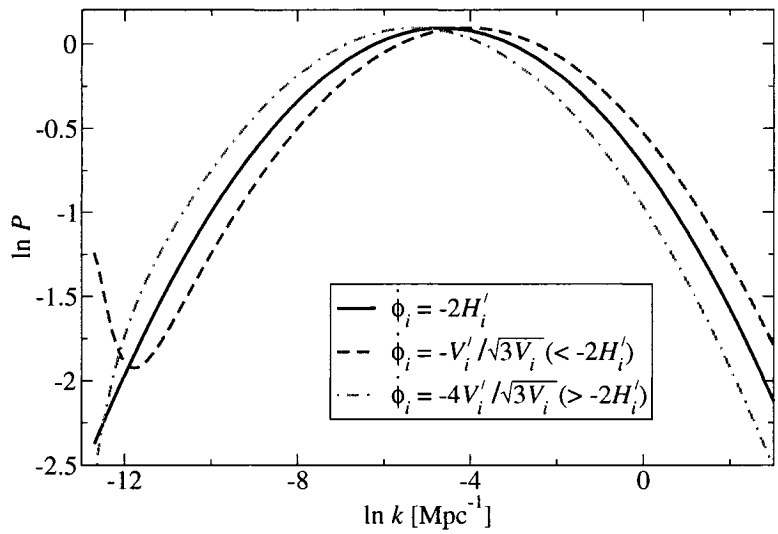

Figure 4.2: The first order reconstructed power spectra for the best fit WMAP running model with different initial inflaton velocities ($n_s = 1.12$, $\alpha_s = -0.076$, $r = 0.24$, and $P_0 = 1$; see column 3b of Table 2.4).

solution [44]. In linear perturbation, the discrepancy between different initial conditions dies away after several e-foldings [36]. Since the late-time behaviors of the inflaton field are asymptotically the same, one does not have to find the "attractor" solution [15]; once we know that a potential with a particular Hubble parameter and $\dot{\phi}_i$ gives the desired properties, *e.g.* power spectrum, we expect a range of initial conditions will also give the same behaviors at late-time. Alternatively, as long as inflation happened at least several e-foldings before today's observable universe passed through the horizon in the early universe, the sensitivity to the initial conditions is damped out.

Chapter 5

Reconstruction: Constant Spectral Index

In this chapter, we investigate the simplest parameterization of the inflationary spectral index which fits the experimental data very well: the case of a constant spectral index, *i.e.* $P = P_0 k^n$, where $P_0 > 0$ and $n \equiv n_s - 1$ are constants. We will see some models where the inflationary trajectories can cross over the boundary $P = H^2$. We also establish the connection between the formulae for spectral indices and the reconstruction of inflaton potentials, and give all analytic potentials for the case of a constant spectral index.

5.1 Particular Potentials

We recover three well-known potentials for the case of a constant spectral index in this section, and present new potentials in the next section.

Power-Law Inflation

Consider the case that n is a non-zero constant. A particular solution is obtained straightforwardly for Eq. (4.9): $H \propto k^{n/2}$. Substituting this particular solution into

Eq. (4.10), one has

$$H = \sqrt{\frac{n}{n-2}P_0}k^{n/2}, \tag{5.1}$$

$$\phi - \phi_0 = \sqrt{\frac{n(n-2)}{2}}\ln\frac{k}{k_0}, \tag{5.2}$$

where ϕ_0 and k_0 are integration constants. ϕ_0 does not have physical significance and hence the scale of k_0 here is arbitrary; we drop them for simplicity in most cases in this and subsequent chapters, but restore them when they are relevant. Note that this solution is valid only for a red tilt ($n < 0$); we will give solutions for a blue tilt ($n > 0$) later.

The reconstructed Hubble parameter and inflaton potential follow directly:

$$H = H_0 \exp\left(-\sqrt{\frac{1}{2p}}\phi\right), \tag{5.3}$$

$$V = \left(3 - \frac{1}{p}\right) H_0^2 \exp\left(-\sqrt{\frac{2}{p}}\phi\right), \tag{5.4}$$

where $p = (n-2)/n = 1/\epsilon > 1$ and $H_0 = \sqrt{P_0/p}$ is the scale of the Hubble parameter and can be fixed by the normalization of the power spectrum. This potential is the power-law ($a \propto t^p$) inflationary potential [45, 35]. As mentioned in Section 3.3, power-law inflation is one example where exact solutions to the original perturbation equations are known [27]. Ref. [46] pointed out that the horizon-crossing/Bessel approximation and the expression for the power spectrum,

$$\mathcal{P}_{\mathcal{R}} \propto \left(\frac{H^2}{\dot{\phi}}\right)^2, \tag{5.5}$$

might fail for non-exponential inflation. However, as shown above, it is interesting that Eq. (5.5) (Eq. (1.21)) is still valid for pure power-law inflation. Therefore, for simplicity, we still use Eq. (1.21) as the basis of the formulation of potential reconstruction.

The number of e-foldings is

$$N = \sqrt{\frac{n-2}{2n}}(\phi_{\text{end}} - \phi). \tag{5.6}$$

Typically, 60 e-foldings are needed for today's observable universe to solve the cosmological problems, $N_* = 60$. In this case, the change in ϕ,

$$\Delta\phi \equiv |\phi_{\rm end} - \phi|, \tag{5.7}$$

is beyond the Planck scale ($1M_{\rm Pl}$) except for very small n. For example, $n \simeq -3\times10^{-4}$ gives $\Delta\phi_* \simeq 1$. Values with subscripts $*$ correspond to $N_* = 60$.

As we will show in Section 5.3 that there is no natural end to inflation in the case of a constant spectral index, we therefore refer to $\phi_{\rm end}$ as the value where inflation is ended by other degrees of freedom or a sudden change in n.

Scale Invariance

Since the power spectrum P is a function of k, Eq. (4.12) cannot be solved directly; however, there is one case where we can solve it without worrying about the horizon crossing condition. It is the case of scale invariance, *i.e.* $P = P_0$ is a constant. The solution of Eq. (1.21) is

$$H = \frac{\sqrt{2P_0}}{|\phi|}, \tag{5.8}$$

$$|\phi| = \left|6\sqrt{2P_0}t\right|^{1/3}. \tag{5.9}$$

The slow-roll parameter is $\epsilon = 2/\phi^2$, so inflation occurs when $|\phi| > \sqrt{2}$. Therefore, if one starts with $0 < t < 1/(3\sqrt{P_0})$, then ϕ will roll from decelerating expansion ($\ddot{a} < 0$) to accelerating expansion (inflation), *i.e.* the inflaton trajectory can cross over the boundary $P = H^2$. The reconstructed potential is

$$V = \frac{6P_0}{\phi^2}\left(1 - \frac{2}{3}\frac{1}{\phi^2}\right). \tag{5.10}$$

This potential is the intermediate (faster than power-law, slower than exponential) inflationary potential with $\beta = 2$ [35, 47, 48]. The general form is

$$H = H_0|\phi|^{-\beta/2}, \tag{5.11}$$

$$V = \frac{3H_0^2}{|\phi|^\beta}\left(1 - \frac{\beta^2}{6}\frac{1}{\phi^2}\right), \tag{5.12}$$

$$a \propto \exp\left(At^f\right), \tag{5.13}$$

where $\beta > 0$ ($\beta < 0$ gives rise to contraction), $0 < f = 4/(\beta + 4) < 1$, and $A = \left[H_0^2/f^2(2\beta)^{\beta/2}\right]^{2/(\beta+4)}$. Figure 5.1 shows the potential corresponding to a scale-invariant spectrum. We emphasize again that only about 10 e-foldings of the reconstructed potential are reliable. Nevertheless, we show wider ranges of the potentials in this chapter to have global descriptions of the potentials. As mentioned in Section 4.1, a more complicated spectral index or other degrees of freedom are needed to make these models realistic.

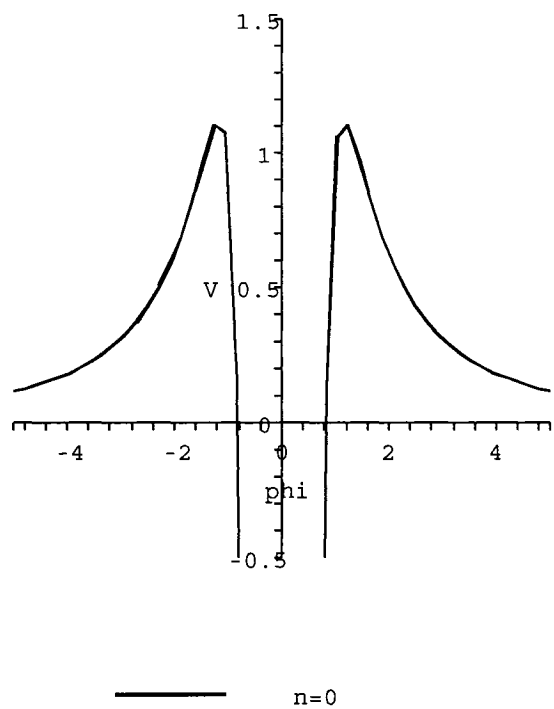

Figure 5.1: The reconstructed potential for a scale-invariant spectrum ($H_0 = 1$).

The number of e-foldings and the change in ϕ are

$$N = \frac{1}{4}\left(\phi_{\text{end}}^2 - \phi^2\right), \tag{5.14}$$

$$\Delta\phi = \sqrt{4N + \phi^2} - |\phi|. \tag{5.15}$$

To have $\Delta\phi_* \sim 1$, we need large $|\phi_*| \sim 10^2$; the absolute value of ϕ, however, does not have physical significance since we have the freedom shift ϕ_0. We will see models which give a nearly scale-invariant spectrum with small inflaton field values and n of

order $O(0.1)$ (remember that to have $\Delta\phi_* \sim 1$ in power-law inflation, $n \sim O(10^{-4})$ is required).

n_s= 3

We find that the first order differential equation, Eq. (4.9), can be reduced to an algebraic equation, which allows us to extend the spectral index to $n > 0$:

$$H^2 - 2P_0k^2 \ln H + Ck^2 = 0, \qquad \text{for } n = 2, \tag{5.16}$$

$$H^n - \frac{n}{n-2}P_0k^nH^{n-2} + Ck^n = 0, \qquad \text{for } n \neq 0, 2, \tag{5.17}$$

where C is an integration constant.

The $n = 2$ case can be solved with the Lambert W function, which satisfies $W(x)\mathrm{e}^{W(x)} = x$. The Hubble parameter and the inflaton field are

$$H = H_0 \exp\left[-\frac{1}{2}W\left(-\frac{C'}{P_0k^2}\right)\right], \tag{5.18}$$

$$\frac{1}{4}\phi^2 = -\frac{1}{2}W\left(-\frac{C'}{P_0k^2}\right), \tag{5.19}$$

where $C' = \exp(C/P_0)$ and $H_0 = \sqrt{C'}$. The irregularities of the Lambert W function in $H(k)$ can be removed if we express H as a function of ϕ:

$$H = H_0 \exp\left(\frac{1}{4}\phi^2\right). \tag{5.20}$$

This model shows that even though the pole exists in the intermediate solution $H = H(k)$ and $\phi = \phi(k)$, it an be removed from the final result $H = H(\phi)$ in some special cases. The reconstructed potential is

$$V = H_0^2\left(3 - \frac{1}{2}\phi^2\right)\exp\left(\frac{1}{2}\phi^2\right). \tag{5.21}$$

This is the $n_s = 3$ case [38]; it is shown in Figure 5.2.

The scale factor cannot be expressed as an analytic function of time, but we have

$$a = a_i\frac{\phi_i}{\phi}, \tag{5.22}$$

$$H_0(t - t_i) = -\int_{\phi_i}^{\phi} \frac{\mathrm{e}^{-\phi^2/4}}{\phi}d\phi \tag{5.23}$$

$$= \mathrm{Ei}\left(1, \frac{1}{4}\phi^2\right) - \mathrm{Ei}\left(1, \frac{1}{4}\phi_i^2\right), \tag{5.24}$$

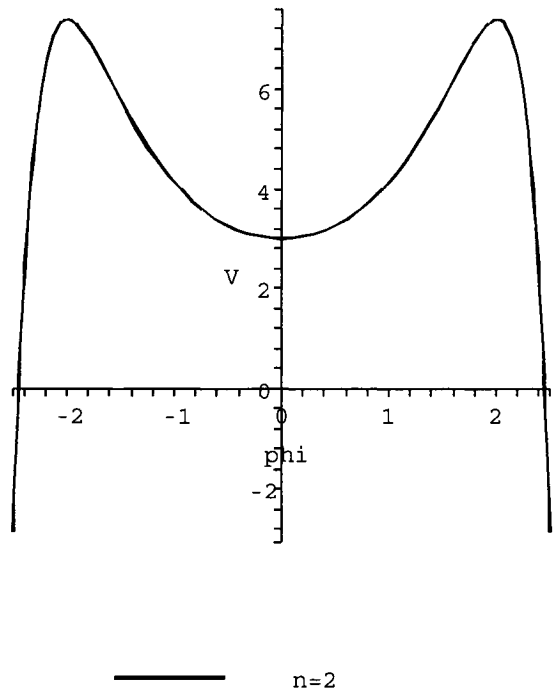

Figure 5.2: The reconstructed potential for a constant spectral index: $n = 2$ ($H_0 = 1$).

where a_i, t_i, and ϕ_i are initial values, and Ei is the exponential integral function:

$$\mathrm{Ei}(a, x) = \int_1^\infty \mathrm{e}^{-xz} z^{-a} dz. \tag{5.25}$$

Inflation occurs when $|\phi| < \sqrt{2}$, and ϕ rolls toward 0 as $t \to \infty$; therefore $\mathrm{e}^{-1/2} < \exp(-\phi^2/4) < 1$ during inflation. Substituting these inequalities into Eqs. (5.23) and (5.22), we have, assuming $t > t_i$,

$$a_i \exp\left[H_0(t - t_i)\right] < a(t) < a_i \exp\left[\mathrm{e}^{1/2} H_0(t - t_i)\right]. \tag{5.26}$$

Therefore, the expansion rate is faster than exponential $a \propto \mathrm{e}^{H_0 t}$. Since one can always have a scale factor expand faster than exponential $\exp(At)$ in a certain range with a sufficiently small A, the above comparison does not have an absolute meaning. Despite this, the constant H_0 represents the energy scale of inflation and can be fixed through the normalization of the power spectrum, so it indeed gives a reference for the expansion rate.

The number of e-foldings is

$$N = \ln\left|\frac{\phi}{\phi_{\rm end}}\right|. \tag{5.27}$$

Therefore, the number of e-foldings is exponentially sensitive to the value of $\phi/\phi_{\rm end}$. If we take, *e.g.*, ϕ_* of order 1, then $\phi_{{\rm end}*}$ has to be fine tuned at the level of $O(10^{-26})$, where inflation ends by other degrees of freedom or by artificially changing the value of n. Nevertheless, since current data suggest a nearly scale-invariant spectrum, we do not take this model with $n_s = 3$ seriously.

5.2 General Solutions

Eq. (5.17) can be solved analytically only when n is a particular rational number, which allows it to be reduced to an algebraic equation with degree smaller than or equal to 4, *e.g.* $n = 1/2, \pm 2/3, \pm 1, 4/3, 3/2, 8/3, \pm 3, \pm 4, \pm 6,$ and 8. Even though one can find $H(k)$, it is not easy to recover $H(\phi)$ analytically. Moreover, if n is an irrational number, Eq. (5.17) cannot be solved analytically at all. Here we introduce a strategy to find general solutions with constant spectral index, which can avoid using the reconstruction equations, Eqs. (4.9) and (4.10).

The formula for the spectral index, Eq. (3.18), can be rewritten as:

$$\eta = \frac{n_s - 1}{2} + \left(2 - \frac{n_s - 1}{2}\right)\epsilon. \tag{5.28}$$

In the case of $n = n_s - 1$ being a constant, it gives a relation between the slow-roll parameters ϵ and η. We can check that all the previous examples satisfy this relation. Moreover, substituting the definitions of the slow-roll parameters, Eq. (5.28) becomes a second order differential equation:

$$\frac{H''}{H} + \left(\frac{n}{2} - 2\right)\left(\frac{H'}{H}\right)^2 - \frac{n}{4} = 0. \tag{5.29}$$

Since this equation is symmetric under $\phi \to -\phi$, if $H(\phi)$ is a solution, $H(-\phi)$ is also a solution. We will see that except for power-law inflation, all other solutions for a constant spectral index are even functions.

Defining $y = \ln H$, Eq. (5.29) becomes

$$y'' + \left(\frac{n}{2} - 1\right) y'^2 - \frac{n}{4} = 0. \tag{5.30}$$

It is a second order, nonlinear differential equation; however, the equation does not explicitly have y- and ϕ-dependent terms, so it can be reduced to a first order differential equation and we can do separating of variables. Defining $z(\phi) = y'$, we have

$$z' + \left(\frac{n}{2} - 1\right) z^2 - \frac{n}{4} = 0. \tag{5.31}$$

If $z' = 0$, then we recover the solution of power-law inflation. For $n = 0, 2$, we recover the solutions in the previous sections.

$0 < n < 2$

If $0 < n < 2$, integrating Eq. (5.31) gives

$$H = H_0 \left| \cos\left[\sqrt{\frac{n(2-n)}{8}}\phi\right] \right|^{2/(n-2)}, \tag{5.32}$$

$$\epsilon = \frac{n}{2-n} \tan^2\left[\sqrt{\frac{n(2-n)}{8}}\phi\right]. \tag{5.33}$$

So inflation occurs when

$$\sqrt{\frac{n(2-n)}{8}}|\phi| < \arctan\left(\sqrt{\frac{2-n}{n}}\right) + m\pi, \tag{5.34}$$

where m is an arbitrary integer and we take $m = 0$ for simplicity. The potential is

$$V = H_0^2 \left| \cos\left[\sqrt{\frac{n(2-n)}{8}}\phi\right] \right|^{4/(n-2)} \left\{ 3 - \frac{n}{2-n} \tan^2\left[\sqrt{\frac{n(2-n)}{8}}\phi\right] \right\}. \tag{5.35}$$

We see that both the Hubble parameter and potential have a period of $2\pi\sqrt{\frac{2}{n(2-n)}}$. Figure 5.3 shows the reconstructed potentials.

The scale factor can be expressed as

$$a = a_i \left\{ \frac{\sin^2\left[\sqrt{n(2-n)/8}\phi_i\right]}{\sin^2\left[\sqrt{n(2-n)/8}\phi\right]} \right\}^{1/n}, \tag{5.36}$$

$$nH_0 t = 2\int_{x_i}^{x} \frac{x^{\frac{4-n}{2-n}}}{1-x^2} dx \tag{5.37}$$

$$= \left(x^2\right)^{\frac{3-n}{2-n}} \Phi\left(x^2, 1, \frac{3-n}{2-n}\right)\Big|_{x_i}^{x}, \tag{5.38}$$

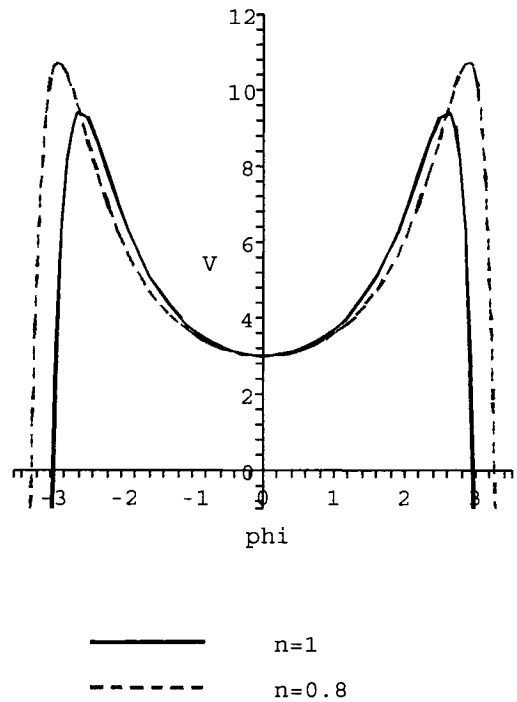

Figure 5.3: The reconstructed potentials for a constant spectral index: $0 < n < 2$ ($H_0 = 1$).

where $x = \cos\left[\sqrt{n(2-n)/8}\phi\right]$ and Φ is the Lerch Φ function:

$$\Phi(z, a, v) = \sum_{m=0}^{\infty} \frac{z^m}{(v+m)^a}. \tag{5.39}$$

Note that during inflation, $H_0 < H < (2/n)^{1/(2-n)} H_0$, which can be seen from Eqs. (5.32) and (5.34), so we have, assuming $t > t_i$,

$$a_i \exp\left[H_0(t - t_i)\right] < a(t) < a_i \exp\left[(2/n)^{1/(2-n)} H_0(t - t_i)\right]. \tag{5.40}$$

This is thus faster than exponential expansion, $e^{H_0 t}$.

The number of e-foldings is

$$N = \frac{2}{n} \ln \left| \frac{\sin\left[\sqrt{n(2-n)/8}\phi\right]}{\sin\left[\sqrt{n(2-n)/8}\phi_{\text{end}}\right]} \right|. \tag{5.41}$$

Similar to the case of $n_s = 3$, we need fine tuning of $\phi_{\text{end}*}$ for $n \to 2^-$. However, for near scale invariance, *e.g.*, $n = 0.1$, $nN_*/2 = 3$, taking $\phi_* = \phi_{\max} \simeq 8.73$, we have

$\phi_{\text{end}*} \simeq 0.315$. To have $\Delta\phi_*$ smaller than the Planck scale, we can set, *e.g.*, $\phi_* = 0.1$, which gives $\phi_{\text{end}*} \simeq 0.005$. We do not need fine tuning and can keep the inflaton field values sub-Planckian; this model is therefore more realistic than the models in the previous sections.

n < 0 or n > 2

Similar to the previous subsection, if $n < 0$ or $n > 2$, the Hubble parameter is

$$H = H_0 \exp\left(\mp\sqrt{\frac{n}{2(n-2)}}\phi\right)\left|1 + C\exp\left(\pm n\sqrt{\frac{n-2}{2n}}\phi\right)\right|^{2/(n-2)}, \tag{5.42}$$

where an arbitrary constant C is introduced to include the particular solution of power-law inflation; however, only the sign of C is relevant since we have the freedom to shift ϕ and rescale H_0. Therefore, we take $C = 0, \pm 1$ for simplicity. To be consistent with the sign convention of power-law inflation, we take the upper signs of $\pm$ or $\mp$. If $C = 1$ and $n = 4$, the Hubble parameter is just a $\cosh(\phi)$ function, which is the case of $A = 1$ in Ref. [49].

The slow-roll parameter ϵ is

$$\epsilon = \frac{n}{n-2}\left[\frac{1 - C\exp\left(n\sqrt{\frac{n-2}{2n}}\phi\right)}{1 + C\exp\left(n\sqrt{\frac{n-2}{2n}}\phi\right)}\right]^2. \tag{5.43}$$

We deduce the following possibilities depending on different combinations of parameters:

1. $C = 0, -1$ and $n > 2 \Longrightarrow \epsilon > 1$: No inflation.

2. $C = 0, 1$ and $n < 0 \Longrightarrow \epsilon < 1$: Eternal inflation.[1]

3. $C = 1$ and $n > 2$: Inflation occurs when

$$|\phi| < \sqrt{\frac{2}{n(n-2)}}\ln\left(\frac{1 + \sqrt{\frac{n-2}{n}}}{1 - \sqrt{\frac{n-2}{n}}}\right). \tag{5.44}$$

[1]We use the terminology "eternal inflation" where inflation occurs for all values of ϕ, $-\infty < \phi < \infty$.

4. $C = -1$ and $n < 0$: Inflation occurs when

$$|\phi| > \sqrt{\frac{2}{n(n-2)}} \ln\left(\frac{\sqrt{\frac{n-2}{n}}+1}{\sqrt{\frac{n-2}{n}}-1}\right). \tag{5.45}$$

The reconstructed potential is

$$\begin{aligned} V &= H_0^2 \exp\left(-\sqrt{\frac{2n}{n-2}}\phi\right)\left|1 + C\exp\left(n\sqrt{\frac{n-2}{2n}}\phi\right)\right|^{4/(n-2)} \\ &\times \left\{3 - \frac{n}{n-2}\left[\frac{1 - C\exp\left(n\sqrt{\frac{n-2}{2n}}\phi\right)}{1 + C\exp\left(n\sqrt{\frac{n-2}{2n}}\phi\right)}\right]^2\right\}. \end{aligned} \tag{5.46}$$

Figures 5.4, 5.5, and 5.6 show the reconstructed potentials.

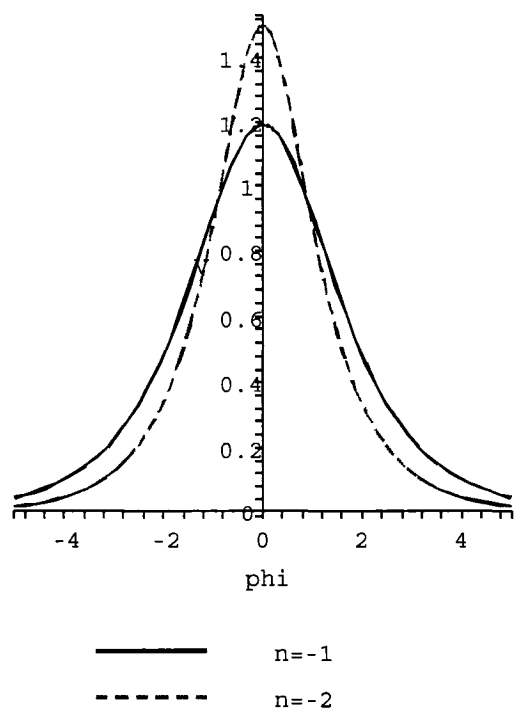

Figure 5.4: The reconstructed potentials for a constant spectral index: $n < 0$ with $C = 1$ ($H_0 = 1$).

The scale factor is

$$a = a_i \exp\left[\sqrt{\frac{n-2}{2n}}(\phi - \phi_i)\right]\left|\frac{1 - C\exp\left(n\sqrt{\frac{n-2}{2n}}\phi_i\right)}{1 - C\exp\left(n\sqrt{\frac{n-2}{2n}}\phi\right)}\right|^{2/n}, \tag{5.47}$$

$$\frac{n}{n-2}H_0 t = \int_{x_i}^{x} \frac{1 + Cx^{n-2}}{1 - Cx^{n-2}}\left|1 + Cx^{n-2}\right|^{-2/(n-2)} dx, \tag{5.48}$$

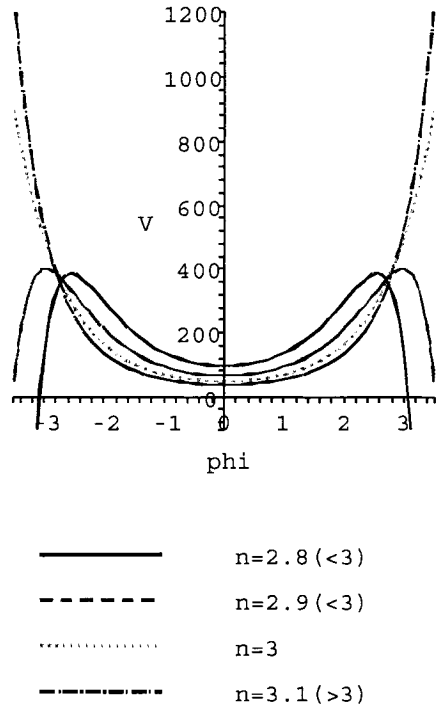

Figure 5.5: The reconstructed potentials for a constant spectral index: $n > 2$ with $C = 1$ ($H_0 = 1$).

where $x = \exp\left[\sqrt{\frac{n}{2(n-2)}}\phi\right]$. If $C = 0$, the scale factor is reduced to power-law expansion ($n < 0$). For other cases, we have (during inflation)

1. $C = 1$ and $n < 0$: $H < 2^{2/(n-2)}H_0$, so $a(t) < \exp\left[2^{2/(n-2)}H_0 t\right] < \mathrm{e}^{H_0 t}$.

2. $C = 1$ and $n > 2$: $H > 2^{2/(n-2)}H_0$, so $a(t) > \exp\left[2^{2/(n-2)}H_0 t\right] > \mathrm{e}^{H_0 t}$.

3. $C = -1$ and $n < 0$: $H < (-2n)^{1/(n-2)}H_0$. Note that $\lim_{n\to 0^-}(-2n)^{1/(n-2)} \to +\infty$ and $\lim_{n\to -\infty}(-2n)^{1/(n-2)} \to 1^-$, so

   (a) $n < -1/2$: $a(t) < \exp\left[(-2n)^{1/(n-2)}H_0 t\right] < \mathrm{e}^{H_0 t}$.

   (b) $n > -1/2$: $\exp\left[(-2n)^{1/(n-2)}H_0 t\right] > \begin{cases} a(t) > \mathrm{e}^{H_0 t}, & \text{if}|\phi| < \sqrt{\frac{2}{n(n-2)}}\ln\left(\frac{3+\sqrt{5}}{2}\right), \\ \mathrm{e}^{H_0 t} > a(t), & \text{if}|\phi| > \sqrt{\frac{2}{n(n-2)}}\ln\left(\frac{3+\sqrt{5}}{2}\right). \end{cases}$

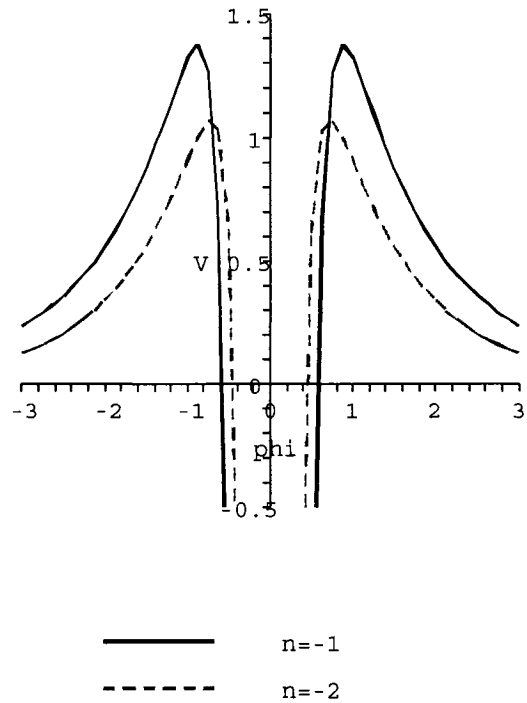

Figure 5.6: The reconstructed potentials for a constant spectral index: $n < 0$ with $C = -1$ ($H_0 = 1$).

The number of e-foldings is

$$N = \sqrt{\frac{n-2}{2n}}(\phi_{\text{end}} - \phi) + \frac{2}{n}\ln\left|\frac{1 - C\exp\left(n\sqrt{\frac{n-2}{2n}}\phi\right)}{1 - C\exp\left(n\sqrt{\frac{n-2}{2n}}\phi_{\text{end}}\right)}\right|. \tag{5.49}$$

If $C = 1$, then the number of e-foldings becomes

$$\exp\left(\frac{nN}{2}\right) = \frac{\sinh\left[\sqrt{n(n-2)/8}\phi\right]}{\sinh\left[\sqrt{n(n-2)/8}\phi_{\text{end}}\right]}. \tag{5.50}$$

If $n \to 0^-$, then $\sinh x_1/\sinh x_2 \simeq x_1/x_2 \simeq \sin x_1/\sin x_2$; it is similar to the case of $0 < n < 2$ when $n \to 0^+$. Otherwise, we need large $\Delta\phi_*$ to give the desired number of e-foldings. If $n \to 2^+$, then $N \sim \ln|\phi/\phi_{\text{end}}|$; we need fine tuning of $\phi_{\text{end}*}$ to give the desired number of e-foldings as in the case of $n_s = 3$.

For $C = -1$, thus $n < 0$, the number of e-foldings is a cosh function:

$$\exp\left(\frac{nN}{2}\right) = \frac{\cosh\left[\sqrt{n(n-2)/8}\phi\right]}{\cosh\left[\sqrt{n(n-2)/8}\phi_{\text{end}}\right]}. \tag{5.51}$$

Again, we need to have n very close to 0^-, *e.g.* $O(10^{-4})$ as in power-law inflation, to give the desired number of e-foldings within sub-Planckian inflaton field values.

5.3 Summary of Constant Spectral Index

Now we have the complete collection of seven independent solutions for the case of a constant spectral index, which cover the entire interval of $-\infty < n < \infty$. Let us consider how the reconstructed potentials depend on the spectral index, and discuss the most realistic model which is consistent with current data.

The Shapes of the Potentials

The shapes of the reconstructed potentials seem to transform continuously from $n < 0$ ($C = -1$, Figure 5.6) to $n = 0$ (Figure 5.1), and from $0 < n < 2$ (Figure 5.3), to $n = 2$ (Figure 5.2) and $n > 2$ (Figure 5.5). However, when $n \to 0^{\pm}$ ($C = -1$), as can be seen from Figures 5.3 and 5.6, both peaks blow up, they do not converge to the case of scale invariance; similarly, when $n \to 2^+$, as can be seen from Figure 5.5, the peaks blow up, it does not converge to the case of $n = 2$. Only when $n \to 2^-$, the potential for $0 < n < 2$ (Figure 5.3) transforms continuously to the case of $n = 2$ (Figure 5.2). Furthermore, two eternal inflationary potentials (power-law inflation and $n < 0$ with $C = 1$) seem to be quite different from other potentials, especially the power-law case, which is the only non-even function.

Three are three solutions for $n < 0$. To break the degeneracy, the slow-roll parameter ϵ is needed:

$$\epsilon \left\{ \begin{array}{c} < \\ = \\ > \end{array} \right\} \frac{n}{n-2} \left\{ \begin{array}{l} C = 1 \\ C = 0 \\ C = -1 \end{array} \right. . \tag{5.52}$$

As can be seen from the slow-roll parameter, Eq. (5.43), and will be proved in general in the next subsection, the ϵ converges to $n/(n-2)$, so these three potentials will converge to the power-law inflationary potential. We can also see from Eq. (5.46) that they have the same asymptotic behaviors at large $|\phi|$, as shown in Figure 5.7.

However, if n is small, *e.g.* $n \simeq -0.01$ [11], then the differences at small $|\phi|$ will become significant.

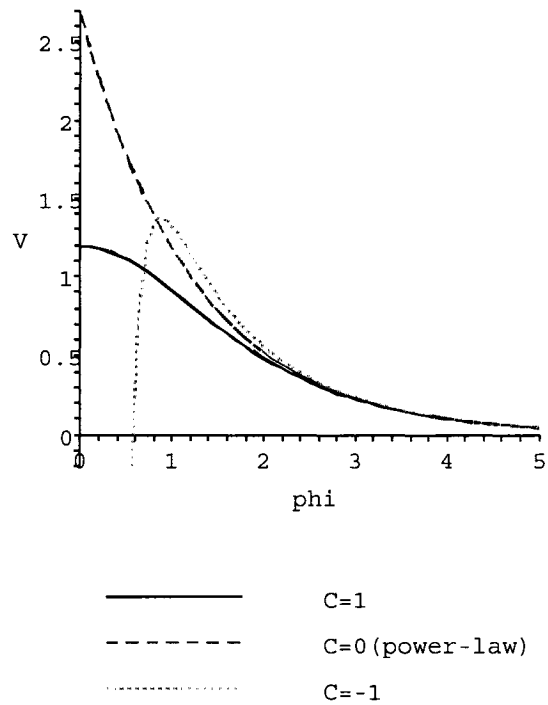

Figure 5.7: Three potentials with $n < 0$ have the same asymptotic behaviors ($n = -1, H_0 = 1$).

So far all potentials we have considered are monotonic during inflation; however, with further investigation, we found that this is not always the case. The Hamilton-Jacobi equation, Eq. (3.3), can be written as

$$V = (3 - \epsilon)H^2. \tag{5.53}$$

From Eqs. (3.12), (3.13), and (3.18), the derivative of the reconstructed potential is

$$V' = HH'[6 - n + (n - 4)\epsilon]. \tag{5.54}$$

Since we assume that the sign of H' does not change during inflation, to have $V' = 0$, we need $n > 6$. Such potentials have local minima, as shown in Figure 5.8. Ref. [49] gives another class of inflationary potentials which also has a similar "Mexican-hat" shape.

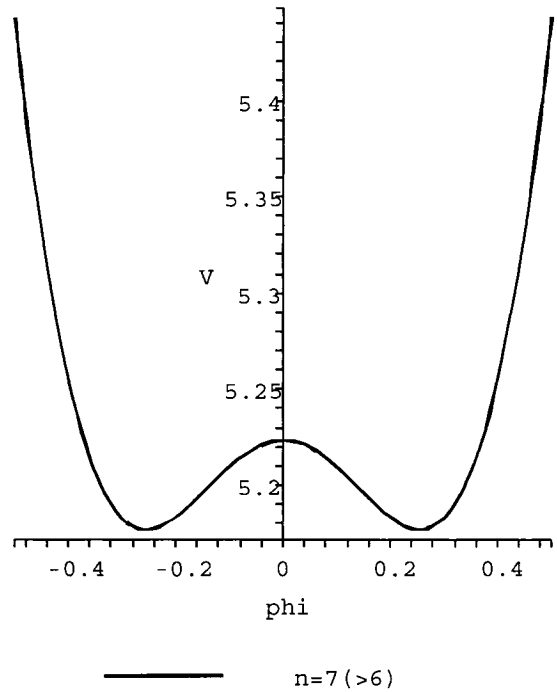

Figure 5.8: The reconstructed potential for a constant spectral index with $n = 7(> 6)$ shows that $V' = 0$ during inflation ($H_0 = 1$).

We must be careful with potentials with large spectral index, since from Eq. (3.18), large n gives rise to large slow-roll parameters hence the slow-roll approximation breaks down. Therefore, our starting point, Eqs. (1.21) and (1.22), would be invalid and some of the previous solutions are not self-consistent. Ref. [50] has argued a potential with large η does not necessarily produce a spectral index predicted by the slow-roll approximation due to the invalidity of the horizon crossing condition. Nevertheless, present data prefer a nearly scale-invariant spectrum [11, 12, 13], so we should not take the solutions with large spectral index seriously.

The End of Inflation and the Scale Factor

From Eqs. (3.13) and (3.18), the derivative of ϵ can be written as

$$\frac{d\epsilon}{d\ln k} = -\frac{\epsilon}{1-\epsilon}[2\epsilon + (1-\epsilon)(n_s - 1)]. \tag{5.55}$$

If $n > 0$, then $d\epsilon/d\ln k < 0$ and it is obvious that $\epsilon \to 0$ as $\ln k \to \infty$. If $n < 0$, then it is easy to show that ϵ will converge to $n/(n-2) < 1$, at which $d\epsilon/d\ln k \to 0$. In both cases, ϵ does not reach 1 at finite $\ln k$ so inflation does not have a natural end for the case of a constant spectral index. As mentioned in Sections 4.1 and 5.1, to make these models realistic, other degrees of freedom must start dominating, or n must change, at some critical point.

As can be seen in the previous sections, the scale factor expands faster than exponential, $e^{H_0 t}$, for blue tilts ($n > 0$), but slower than exponential for $n \leq 0$; here H_0 is the normalization factor, which sets the lower bound for the Hubble parameter during inflation in the case of blue tilt, and the upper bound in the case of $n \leq 0$. There is an exception, $-1/2 < n < 0$ with $C = -1$, where H_0 is neither a lower nor an upper bound.[2] Note that H_0 varies between different models, so different models cannot be compared directly.

The Best Fit Non-Running Potential

Usually, we need to fine tune $\phi_{\text{end}*}$ ($n > 0$ and $n < 0$ with $C = 1$) or large $\Delta\phi_*$ (power-law inflation, scale invariance, and $n < 0$ with $C = -1$) to give the desired number of e-foldings. The only case where we can avoid the fine tuning problem and keep all relevant scales sub-Planckian is the nearly scale-invariant case, *e.g.* $n \sim 0.1$ (we do not need to tune n to be very small, $O(10^{-4})$, as required in power-law inflation and $n < 0$ with $C = -1$). Two potentials have this property; they are the eternal inflation ($C = 1$) and the $0 < n < 2$ case. In both cases, the slow-roll parameter is

$$\epsilon \sim \frac{n^2}{8}\phi^2, \qquad \text{for } n \to 0. \tag{5.56}$$

Therefore, they have the extra nice property that the slow-roll approximation is well satisfied (η automatically satisfies the condition; see Eq. (5.28)). This is important because the validity of Eq. (1.21) is based on the slow-roll approximation; thus a self-consistent solution is required.

[2]Power-law inflation is not included this analysis.

Since current data prefer a red-tilted spectral index, the eternal inflation case ($C = 1$) represents our best fit non-running potential. The best fit spectral index for the non-running model is $n = -0.05$ from the three-year WMAP data; see column 3a of Table 2.1. To keep $\Delta\phi_*$ small, we take, *e.g.*, $\phi_i = 0.1$, then we have 60 e-foldings at $\phi_{\text{end}*} \simeq 0.45$.[3] The slow-roll parameter ϵ is of order 10^{-5} and η is about -0.025 in this range, so the slow-roll approximation is well satisfied and hence the second order corrections are completely negligible. Furthermore, a small ϵ implies a low tensor-to-scalar ratio, $r = 16\epsilon < 10^{-3}$, so this model is consistent with the best fit non-running model where the tensor spectrum is ignored. Since the slow-roll parameter is small, $\epsilon \sim 10^{-5}$, the energy scale is described by the COBE normalization [6]: $V^{1/4} \simeq 0.027\epsilon^{1/4} M_{\text{Pl}} \simeq 3.7 \times 10^{15}\text{GeV}$.

In brief, a slow-roll inflationary potential can give rise to a nearly scale-invariant spectrum, which can sustain inflation for 60 e-foldings within sub-Planckian inflaton field values at the potential energy scale of order $V^{1/4} \sim 10^{15}\text{GeV}$; the tensor-to-scalar ratio is negligible as is so far consistent with experiments. However, there is no natural end to inflation; other degrees of freedom are needed for a consistent realization of this model.

[3]We need an extra condition, *e.g.* the tensor-to-scalar ratio r, to fix the value of ϕ_i (or the overall scale). Here we choose a small ϕ_i to keep $\Delta\phi_*$ small. Nevertheless, different extra conditions just affect the overall factor of the potential; its shape does not change. See the discussion in Section 6.1.

Chapter 6

Reconstruction: Running Spectral Index

It is always possible to expand the power spectrum around a pivot point, k_0:

$$\ln P(k) = \ln P(k_0) + n \ln(k/k_0) + \frac{1}{2}\alpha_s \ln^2(k/k_0) + \frac{1}{3!}\frac{d^2 n_s}{d\ln k^2}\bigg|_{k=k_0} \ln^3(k/k_0) + \ldots \quad (6.1)$$

where $n = n_s(k_0) - 1$ and $\alpha_s = dn_s/d\ln k|_{k=k_0}$ are denoted as the values of the spectral index and its running at the pivot point in this chapter. In last chapter we discussed the case of a constant spectral index, which keeps only the linear term in the above expansion; in this chapter, we explore the second simplest case, a parabolic power spectrum, *i.e.*, $\alpha_s \neq 0$ but higher order terms are dropped. This parameterization can give a slightly better fit to the data, as discussed in Section 2.2.

6.1 Unique Solution?

Here we use the same strategy as in Section 5.2 to see if we can find analytic solutions for the case of a running power spectrum. Similarly, defining $y(\phi) = \ln H$, the formula for the running of the spectral index, Eq. (3.20), becomes

$$y'''y'\left(y'^2 - \frac{1}{2}\right) + y''y'^2\left(1 - 2y''\right) + \frac{\alpha_s}{2}\left(y'^2 - \frac{1}{2}\right)^3 = 0. \quad (6.2)$$

To reduce the order of the above equation, we define $z(\phi) = y'$:

$$z''z(z^2 - \frac{1}{2}) + z'(1 - 2z')z^2 + \frac{\alpha_s}{2}(z^2 - \frac{1}{2})^3 = 0. \tag{6.3}$$

Defining $p(z) = z'$ will further reduce the order of the equation:

$$pz\left(z^2 - \frac{1}{2}\right)\frac{dp}{dz} + pz^2(1 - 2p) + \frac{\alpha_s}{2}\left(z^2 - \frac{1}{2}\right)^3 = 0. \tag{6.4}$$

Setting $\alpha_s = 0$ in the above equation, we recover all constant spectral index solutions. This is the Abel differential equation; defining $u = 1/p$ brings it back to the usual form. Some classes of the Abel differential equations have analytic solutions, but our equation seems to be in the class whose solutions remain unknown;[1] thus we do not have analytic solutions for the running spectral index model at present.

To numerically solve the differential equations of potential reconstruction, Eqs. (4.9) and (4.10), a set of initial conditions is needed:

$$\begin{cases} H(k_i) &= H_i, \\ \phi(k_i) &= \phi_i. \end{cases} \tag{6.5}$$

Since we have the freedom to shift the inflaton field, we set $\phi_i = 0$ for simplicity. The value of H_i determines the value of ϵ_i because $\epsilon = H^2/P$. So the initial conditions, Eq. (6.5), are just the values of (k_i, ϵ_i). Now, a question arises: Do different initial conditions give different Hubble parameters, or the same Hubble parameter with different normalization factors? To answer this equation, we first investigate the case of a constant spectral index where we have analytic solutions, and then discuss the case of a running spectral index.

We assume that for a given power spectrum and initial conditions, the solution can be written as

$$H(\phi) = H_0 h(\phi), \tag{6.6}$$

where H_0 is an overall factor and there is no arbitrary constant in $h(\phi)$. Now, we recover the integration constant ϕ_0, which was dropped in Chapter 5, and we will

[1] Maple 9 claims that it incorporates most solvable Abel classes known by 2000, but it does not give a solution for Eq. (6.4).

soon see that it is relevant. Together with the expression of the power spectrum, Eq. (1.21) (remember that $P = 8\pi\mathcal{P}_{\mathcal{R}}$), and the initial conditions, Eq. (6.5), we have

$$P(k_i) = \frac{1}{2}H_i^2\left[\frac{h(-\phi_0)}{h'(-\phi_0)}\right]^2, \tag{6.7}$$

$$H_i = H_0 h(-\phi_0). \tag{6.8}$$

We see that Eq. (6.7) determines ϕ_0, which represents the initial value of ϕ (corresponding to k_i), and Eq. (6.8) fixes H_0, which is the overall factor. Therefore, different choices of initial conditions, (k_i, ϵ_i), just give different values of ϕ_0 and $V_0 = H_0^2$, but the shapes of the Hubble parameter, $h(\phi)$, and potential, $(3-\epsilon)h(\phi)^2$, remain unchanged.

Since we have obtained all the analytic solutions for the case of a constant spectral index, we can check that different initial conditions just give different values of H_0 and ϕ_0, but $h(\phi)$ is uniquely determined by the spectral index. The reason why we have unique solutions for the case of a constant spectral index is because Eq. (5.31) is a first order equation, so a single initial condition, $\epsilon_i = 2z_i^2$, determines $h(\phi)$ uniquely.

In the case of a running spectral index, Eq. (6.3) is a second order equation of z, so we need both z_i and z_i'. From Eqs. (3.12), (3.13), and (3.18), one has

$$\epsilon' = \frac{H'}{H}\left[2\epsilon + (1-\epsilon)(n + \alpha_s \ln\frac{k}{k_0})\right], \tag{6.9}$$

$$z' = \frac{\epsilon'}{4z} = \frac{1}{4}\left[2\epsilon + (1-\epsilon)(n + \alpha_s \ln\frac{k}{k_0})\right]. \tag{6.10}$$

Assume that we have solutions, H_1 and H_2, for the reconstruction equations Eqs. (4.9) and (4.10) with initial conditions (k_i, ϵ_{1i}) and (k_i, ϵ_{2i}). When we evaluate $H_1(k)$ at $k_i' \neq k_i$, at which $\epsilon_1(k_i') = \epsilon_{2i}$, we will have $\epsilon_1'(k_i') \neq \epsilon_2'(k_i)$ according to Eq. (6.9). Therefore, h_1 and h_2, which determine ϵ_1 and ϵ_2, are different solutions.

Since different initial conditions give rise to different shapes of the Hubble parameter, let us see how the Hubble parameter and other physical quantities vary with ϵ_i. Since H is always decreasing, H_i would set the overall scale for the Hubble parameter ($\sim H_i$) and the potential ($\sim H_i^2$). Also, from Eq. (4.10) we see that $\Delta\phi$ scales as H_i. Consider the case that ϵ_i is small; we expect that $|\Delta H| \sim |H'\Delta\phi| = H|\Delta\phi|\sqrt{\epsilon/2}$ does

not change much in a small range of $\Delta\phi$ (or $\Delta \ln k$). So the expansion rate goes like

$$a \sim \mathrm{e}^{H_i t}, \tag{6.11}$$

and the number of e-foldings is

$$N = \ln \frac{a}{a_i} = \ln \frac{k}{k_i} + \ln \frac{H_i}{H} \gtrsim \ln \frac{k}{k_i}. \tag{6.12}$$

In brief, we can tune ϵ_i to be very small to have both the inflaton potential and $\Delta\phi$ much smaller than the Planck scale; the cost is a low expansion rate (and a low tensor-to-scalar ratio because of the small ϵ). The number of e-foldings, however, is approximately unchanged over a small range of $\ln k$. For example, for the cosmologically interesting scales, $10^{-4} < k(\mathrm{Mpc}^{-1}) < 1$, the number of e-foldings is approximate 9.2.

6.2 Tensor Spectrum

In the last section we argued that different values of ϵ_i give different shapes for the Hubble parameter in the case of a running spectral index; to uniquely determine the Hubble parameter, and hence the inflaton potential, we have to choose a particular ϵ_i. In fact, this is fixed by the tensor-to-scalar ratio, Eq. (3.22). In this section, we discuss the consequences of using different tensor spectra.

The tensor spectrum is not as well determined as the scalar spectrum, and its running is too weak to be detected at present. Therefore, it is sufficient to parameterize the tensor spectrum as

$$\mathcal{P}_h = \mathcal{P}_{h0} k^{n_t}, \tag{6.13}$$

where n_t is a constant. As mentioned in Section 4.1, one can also reconstruct the Hubble parameter from the tensor spectrum. Substituting the parameterization, Eq. (6.13), into the tensor reconstruction equations, Eqs. (4.7) and (4.8), one has the solution:

$$H = \frac{\sqrt{P_{h0}}}{4} \exp\left(\mp\sqrt{\frac{n_t}{2(n_t-2)}}\phi\right), \tag{6.14}$$

where $P_{h0} = 8\pi^2\mathcal{P}_{h0}$. Comparing this result with the power-law solution, Eq. (5.3), we have

$$n_t = n, \tag{6.15}$$

$$\mathcal{P}_h(k) = \frac{16}{p}\mathcal{P}_{\mathcal{R}}(k), \tag{6.16}$$

where $p = (n-2)/n = \epsilon^{-1}$; see Section 5.1. Note that this result is consistent with the exact result in both the amplitude ratio and the spectral indices [27].

One can see from the above that a non-running tensor spectrum corresponds to power-law inflation, which has a constant scalar spectral index; therefore, parameterizing a running scalar index and a non-running tensor spectral index, as the WMAP collaboration do, is not self-consistent. Once a scalar spectrum and a tensor-to-scalar ratio are given, the tensor spectrum can be determined uniquely through the Hubble parameter. Figure 6.1 shows the best fit WMAP parabolic scalar spectrum (solid, black; see column 3b of Table 2.4), its reconstructed tensor spectrum (dashed, red), and the tensor spectrum reconstructed from the inflationary consistency equation (dot-dashed, green), Eq. (1.39):

$$\ln P_h = \ln\left[rP_0 e^{n_t \ln(k/k_0)}\right] \simeq \ln(rP_0) - (r/8)\ln(k/k_0). \tag{6.17}$$

Since at cosmologically interesting scales the slow-roll parameters are small (see Section 6.3, Figure 6.4), the inflationary consistency equation is a good approximation, as can be seen in Figure 6.1. Consequently, the present data does not discriminate between different parameterizations of the tensor spectrum [25]. Nevertheless, using a self-consistent tensor spectrum requires neither an extra parameter nor a complicated algorithm, so it should be considered in future data fitting.

As for the reconstruction of a running tensor spectral index,

$$\ln P_h = \ln P_{h0} + n_t \ln(k/k_0) + \frac{1}{2}\alpha_t \ln^2(k/k_0), \tag{6.18}$$

we can also solve Eq. (4.8) directly, which gives $\phi = \phi(\ln k)$; or solve the running equation Eq. (3.21), which gives $\phi = \phi(H'/H)$. In any case, it seems that we do not have analytic expressions for $H = H(\phi)$ for a running tensor spectral index.

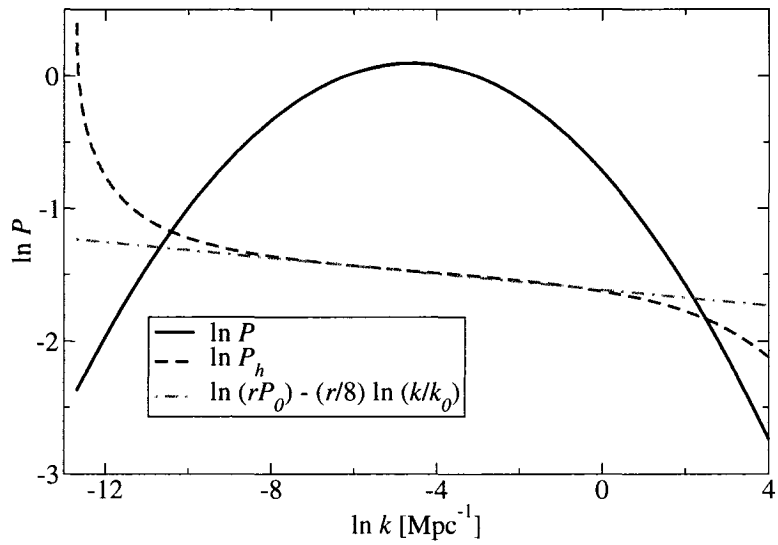

Figure 6.1: The tensor spectra reconstructed from the scalar spectrum and from the inflationary consistency equation ($r(k_0) \simeq 0.24, P_0 = 1$).

6.3 WMAP Running Power Spectrum

In this section, we reconstruct the inflaton potential from the best fit WMAP running spectral index, and discuss some theoretical aspects.

The three-year WMAP running power spectrum is given in column 3b of Table 2.4 ($k_0 = 0.002\text{Mpc}^{-1}$):

$$n = 0.12, \qquad \alpha_s = -0.076, \tag{6.19}$$

with the tensor-to-scalar ratio:

$$r = 0.24. \tag{6.20}$$

Figure 6.2 shows the reconstructed Hubble parameter and inflaton potential. Here we emphasize that one has the freedom to choose the constant ϕ_0, and hence the values of the inflaton field do not have absolute meanings.

The second order corrections (see Section 4.2) are not significant because the slow-roll parameters are small at the relevant scales; see Figure 6.4. Although the slow-roll parameters become large at late times, they do not have much effect on the power spectrum. This is because $n_s - 1 = n + \alpha_s \ln(k/k_0) < 0$ at late times, hence ϵ

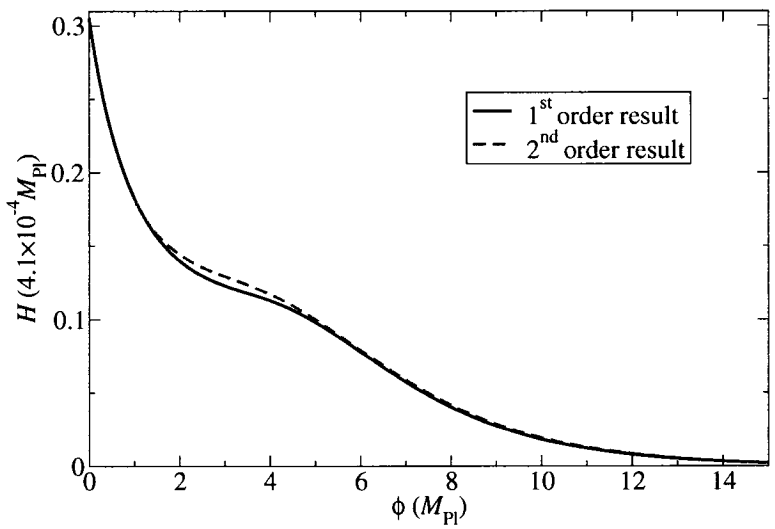

(a)

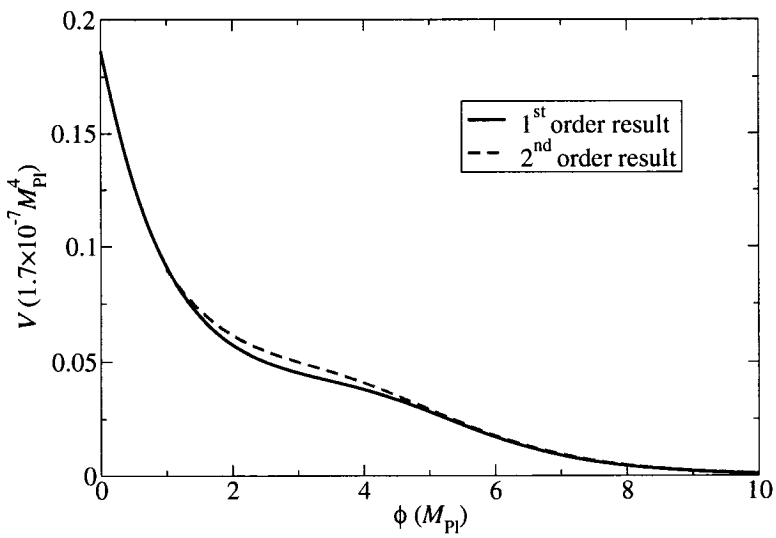

(b)

Figure 6.2: The reconstructed Hubble parameter (a) and inflaton potential (b) for the best fit WMAP running model ($P_0 = 1$).

converges to $(n_s - 1)/(n_s - 3)$ according to Eq. (5.55);[2] together with Eq. (5.28), one finds that η will also converge to $(n_s - 1)/(n_s - 3)$, therefore, the correction factor in Eq. (3.25) reads:

$$[1 - \epsilon + (2 - \ln 2 - \gamma)(2\epsilon - \eta)]^2 \simeq (1 - 0.27\epsilon)^2. \tag{6.21}$$

So the second order corrections remain insignificant even though the slow-roll parameters are large. In fact, the main reason why the corrections are small is that we keep the same H_i in each iteration;[3] this is actually equivalent to choose a particular initial condition in the higher order differential equation, Eq. (4.19), to make the corrections small.

As for the inflationary energy scale, we need to restore the normalization factor of the power spectrum, 2.2×10^{-9} (column WMAP3b of Table 2.4), and the $8\pi^2$ factor we have dropped; the units for Figures 6.2 (a) and (b) are $4.1\times10^{-4}M_{\rm Pl}$ and $1.7\times10^{-7}M_{\rm Pl}^4$ respectively. So at the pivot point ($\phi \simeq 3.06M_{\rm Pl}$), $H \simeq 5.1\times10^{-5}M_{\rm Pl} \simeq 1.2\times10^{14}$GeV and $V^{1/4} \simeq 9.4 \times 10^{-3}M_{\rm Pl} \simeq 2.3 \times 10^{16}$GeV. Since the slow-roll parameter is small at the pivot point, $\epsilon(k_0) = r(k_0)/16 = 0.015$, this energy scale is consistent with the COBE normalization result [6]: $V^{1/4}(k_0) \simeq 0.027\epsilon^{1/4}(k_0)M_{\rm Pl} \simeq 2.3 \times 10^{16}$GeV.

Figure 6.3 shows the logarithm of the scale factor as a function of time. We see that the scale factor expands exponentially and then turns to a power-law expansion rate. For the cosmologically interesting scales, $10^{-4} < k(\mathrm{Mpc}^{-1}) < 1$, we have 9.4 e-foldings (a little bigger than number predicted by Eq. (6.12)), in which the scale

[2]As mentioned in Section 5.3, ϵ always remains less than 1 in the case of a constant spectral index; for a running spectral index, although ϵ still converges to $(n_s - 1)/(n_s - 3)$ for $n_s < 1$, since $n_s - 1 = n + \alpha_s \ln(k/k_0)$ is not a constant, it is possible for ϵ to reach 1 at finite $\ln k$. However, it is impossible to see this effect when numerically solving the reconstruction equations, Eqs. (4.9) and (4.10).

[3]According to Eq. (5.28), if $\epsilon = 1^-$ ($\ln k_i[\mathrm{Mpc}^{-1}] = -12.7$), then $\eta = 2$, so the correction factor in Eq. (3.25) is 0, and the iteration method introduced in Section 4.2 fails. We choose a slightly larger initial value, $\ln k_i'[\mathrm{Mpc}^{-1}] = -12.2$, for the second order corrections to avoid this problem; see the following discussion about the numbers.

factor can be parameterized as exponential expansion:

$$a \sim \mathrm{e}^{0.12t} \simeq \exp\left[5 \times 10^{-5} t(M_{\mathrm{Pl}}^{-1})\right] \simeq \exp\left[1.8 \times 10^{38} t(\mathrm{s})\right], \tag{6.22}$$

where we have restored the normalization factor for the Hubble parameter, $4.1 \times 10^{-4} M_{\mathrm{Pl}}$.[4] So we have 9.4 e-foldings within 5.1×10^{-38} seconds. Note, since ϵ_i is not small, the scale factor does not scale as $\mathrm{e}^{H_i t}$ ($H_i \simeq 0.31$).

Since ϵ is always smaller than 1, it seems that we can have as many e-foldings as we want. However, the slow-roll parameters are increasing at large $\ln k$, so the slow-roll approximation breaks down before we have 60 e-foldings. For example, we can only have about 19 e-foldings while $\epsilon < 0.2$ in our running spectrum case, as shown in Figure 6.4. In addition, we can only extend the Hubble parameter to k_{min}, at which $\epsilon = 1^-$ and the reconstruction equations, Eqs. (4.9) and (4.10), break down. In our case, $\ln k_{\mathrm{min}}[\mathrm{Mpc}^{-1}] \simeq -12.7$ when requiring $r(k_0) \simeq 0.24$. Consequently, as can be seen from Figure 6.4, the slow-roll parameters are quite large within cosmologically interesting scales; for instance, the lowest value of $\ln k$ [Mpc^{-1}] called by CosmoMC is about -12. The large value of ϵ is because we require large value of tensor-to-scalar ratio.

Therefore, if slow-roll inflation is expected to give about 60 e-foldings, then some assumptions we have made may break down, and we may need to consider other possibilities, like:

1. There is more than one dynamical degree of freedom, *i.e.* multiple-field inflation.

2. A spectrum with large running and tensor-to-scalar ratio is valid only for about 10 e-foldings; we should not extend it to large k (unobservable) region.

An alternative way to solve the above problem is the partial running spectrum, which will keep the slow-roll parameters small and does not change other best fit cosmological parameters (see discussion in Section 2.2). With a low-k cutoff on the running of the spectrum, the beginning of slow-roll inflation can be pushed far before

[4] $1 M_{\mathrm{Pl}} = 3.7 \times 10^{42} \mathrm{s}^{-1}$; see Appendix A.

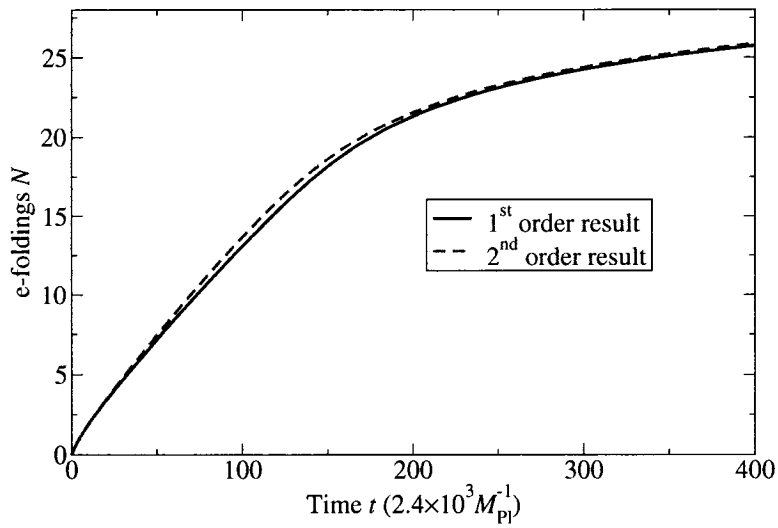

(a)

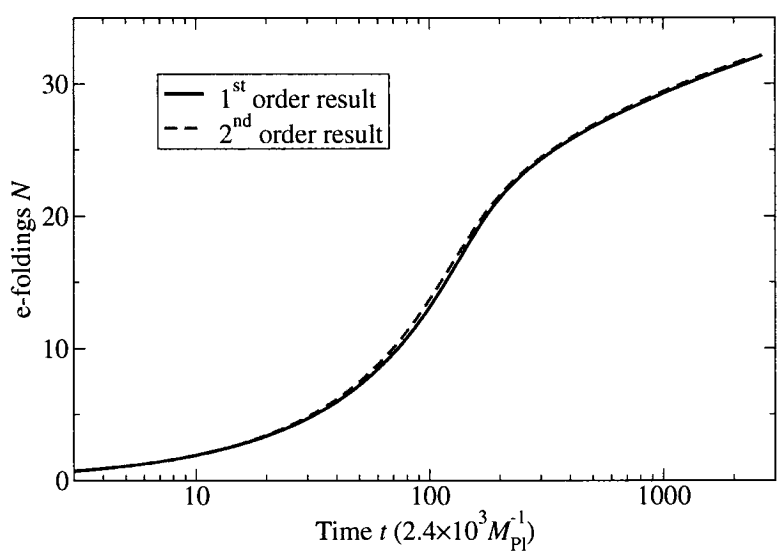

(b)

Figure 6.3: The logarithm of the scale factor as a function of time reconstructed from the best fit WMAP running model.

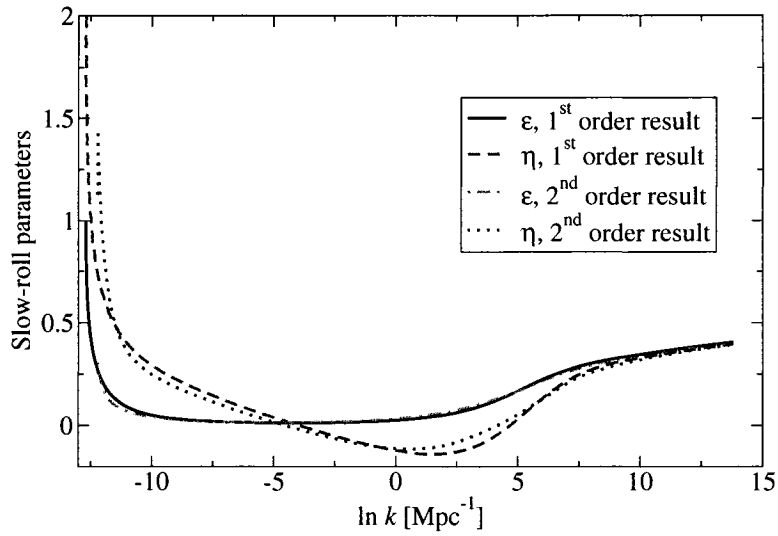

Figure 6.4: The reconstructed slow-roll parameters for the best fit WMAP running model.

today's cosmologically interesting scales, while maintaining a large tensor-to-scalar ratio at the pivot point. Figure 6.5 shows the WMAP partial running model (see column WMAP3b of Table 2.6), where the slow-roll parameters are seen to remain small during the relevant part of inflation. The discontinuity in η is due to the discontinuity in the slope of the power spectrum where it goes between non-running and running, which could be avoided by making a smoother transition. Figure 6.6 shows the reconstructed potential for the WMAP partial running spectrum. Since the power spectrum is set to be flat in the low- and high-k parts, this potential is just a combination of the running potential in the middle and the scale-invariant potential, Eq. (5.10), at both ends. As mentioned in Section 5.1, a super-Planckian field value is needed to give 60 e-foldings in this scale-invariant potential.

From the perspective of particle physics model-building, it is interesting to see if the reconstructed potential for a large running power spectrum can be described by a renormalizable potential. We have therefore fit the reconstructed V to a quartic polynomial for different ranges of field values. Figure 6.7 shows the fitting from $\ln k_i = -9.2$ (10^{-4} Mpc^{-1}) to $\ln k_f = 0$ (1 Mpc^{-1}), 3.8, 4.8, and 5.8, obtaining fits

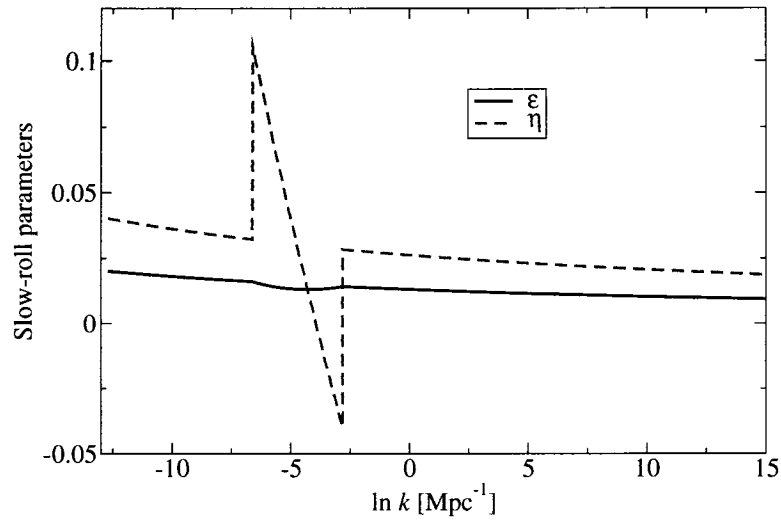

Figure 6.5: The reconstructed slow-roll parameters for the WMAP partial running model.

which for the case of $\ln k_f = 4.8$ has the form

$$V = 1.7 \times 10^{-7} \times (0.0510 - 0.0125\phi + 0.00623\phi^2 - 0.00277\phi^3 + 0.000357\phi^4). \quad (6.23)$$

To better discriminate the goodness of fit, we also plot the fractional errors in Figure 6.8. We see that final k values up to $\ln k_f = 4.8$ provide good fits at the percent level. This $\ln k_f$ value corresponds to 15 e-foldings from $k = 10^{-4}\text{Mpc}^{-1}$. Although the inflaton changes by super-Planckian values, the smallness of the coefficients in the renormalizable potential indicates that the effective field theory description for a large running power spectrum is not invalidated, because higher order terms give smaller contributions to V, even at $\phi = 7M_{\text{Pl}}$.

To summarize this section, the best fit WMAP running model gives rise to a potential with energy scale $V^{1/4} \sim 10^{16}\text{GeV}$, where super-Planckian inflaton field values are needed to obtain 60 e-foldings. Despite this, the smallness of the coefficients of the potential implies that the effective field theory is still a good description.

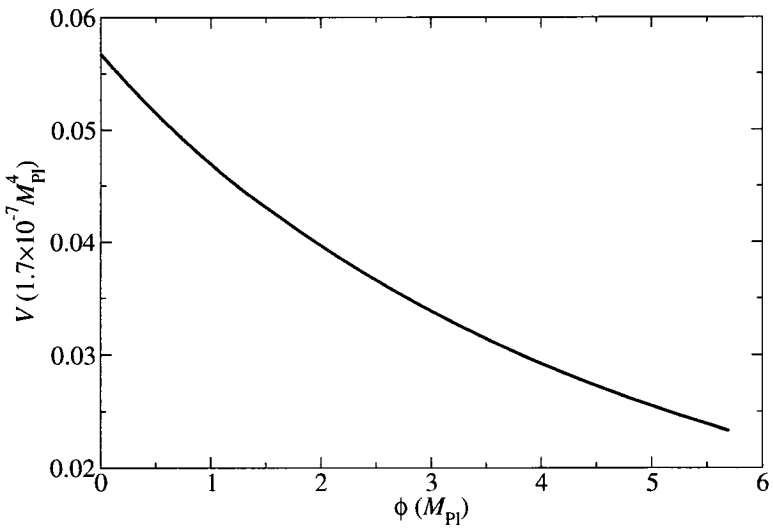

Figure 6.6: The reconstructed potential for the WMAP partial running model.

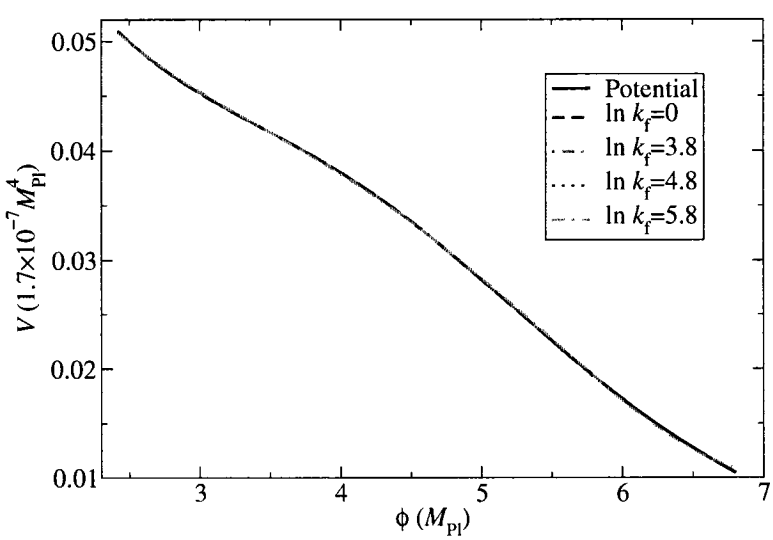

Figure 6.7: The reconstructed potential for the best fit WMAP running model and a series of renormalizable potentials fitting over different ranges of field values.

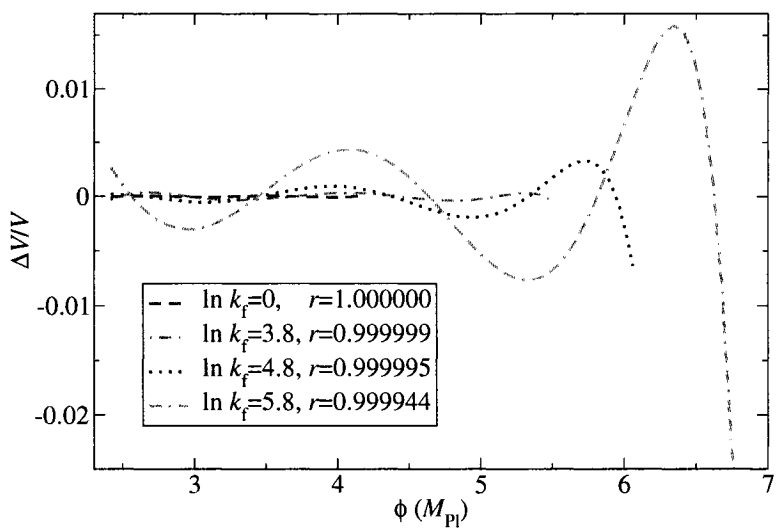

Figure 6.8: The fractional errors of the fitting potentials. The correlation coefficient r for each fit is also shown.

Chapter 7

Conclusions

Inflation has become one of the cornerstones of modern cosmology; it not only solves the critical cosmological problems, but also provides possibilities to explore the infant universe. One of the important aspects of inflationary theory is the primordial power spectrum, which connects the quantum fluctuations in the early universe and the formation of structure of the present universe. In this thesis, we discussed both experimental and theoretical aspects of the inflationary power spectrum.

We studied the experimental evidence for the six-parameter cosmological model, which has a nearly scale-invariant spectral index and fits the current data very well. We also investigated the question of the large running of the inflationary spectral index in the light of recent WMAP data. By exploring the WMAP data multipole by multipole, we found that the evidence for running mainly comes from multipoles near $l = 40$. This perspective lends more interest to the possible confirmation or negation of large running by future improvements in the data, since the experimental determination of the higher multipoles is not so limited by cosmic variance. Moreover, this fact allows us to adjust the shape of the power spectrum, and we found that a partial running spectrum gives as good a fitting as the full running spectrum.

We gave some simple formulae of the inflationary spectral indices based on the Hamilton-Jacobi formulation of inflation. These formulae are the exact results to the leading order of the slow-roll approximation of the power spectra; nevertheless, they do reproduce the predictions given by some exact solutions of the original perturbation

equations of the power spectra. Although there exist higher order results in the slow-roll approximation for the inflationary spectral indices, none of them can reproduce the predictions given by the original exact solutions. Therefore, our simple formulae remain interesting in some special cases.

The Hamilton-Jacobi formulation of inflation was also applied to reconstruct inflationary potentials from a given power spectrum. A simple and accurate reconstruction formulation was presented. Some well known potentials for constant spectral index were recovered; new potentials for constant spectral index were also derived, which show that a nearly scale-invariant spectrum can give rise to slow-roll inflation during 60 e-foldings within sub-Planckian inflaton field values and a potential energy $V^{1/4} \sim 10^{15}$GeV. Potentials for large running of spectral index and large tensor-to-scalar ratio were also constructed, and they need super-Planckian field values but sub-Planckian potential energy, $V^{1/4} \sim 10^{16}$GeV. For these, the slow-roll approximation breaks down before reaching 60 e-foldings. This problem, however, can be solved by the partial running model. We have shown that for the cosmologically interesting scales, a renormalizable potential fits the reconstructed potential for a large running spectral index very well. Therefore the effective field theory description does not break down at inflationary energy scales.

Our reconstruction method also provides a simple algorithm to find a self-consistent tensor spectrum once a scalar spectrum and a tensor-to-scalar ratio are given. Although we mainly discussed the leading order results of the slow-roll approximation in this thesis, we also showed that higher order corrections can be straightforwardly incorporated into the formulae of spectral indices and the reconstruction formulation.

Appendix A

Units and Constants

We use natural units in this thesis, where the speed of light c, the reduced Planck constant $\hbar$, and the Boltzmann constant k_{B} are set to 1. In this system, the basic dimension is energy, 1GeV. The conversion between natural units and international units is [6]

$$\begin{aligned}
1\mathrm{cm} &= 5.068 \times 10^{13}\mathrm{GeV}^{-1}\hbar, \\
1\mathrm{s} &= 1.519 \times 10^{24}\mathrm{GeV}^{-1}\hbar/c, \\
1\mathrm{g} &= 5.608 \times 10^{23}\mathrm{GeV}/c^2, \\
1\mathrm{K} &= 8.618 \times 10^{-14}\mathrm{GeV}/k_{\mathrm{B}}.
\end{aligned}$$

We also set the reduced Planck mass to 1, and hence all quantities have the same dimension. The value of the reduced Planck mass is [6]

$$1M_{\mathrm{Pl}} = 2.436 \times 10^{18}\mathrm{GeV}.$$

Bibliography

[1] A. H. Guth, "Inflationary Universe: A Possible Solution to the Horizon and Flatness Problems," Phys. Rev. **D 23**, 347 (1981).

[2] P. J. E. Peebles, "Principles of Physical Cosmology," Princeton University Press, Princeton (1993).

[3] J. A. Peacock, "Cosmological Physics," Cambridge University Press, Cambridge (1999).

[4] A. R. Liddle, "An Introduction to Cosmological Inflation," in "1998 Summer School in High Energy Physics and Cosmology," 260, A. Masiero, G. Senjanovic, and A. Smirnov (editors), World Scientific, Singapore (1999) [arXiv:astro-ph/9901124].

[5] R. H. Brandenberger, "Inflationary Cosmology: Progress and Problems," in "Large Scale Structure Formation," 169, R. Mansouri and R. Brandenberger (editors), Kluwer Academic Publishers, the Netherlands (2000) [arXiv:hep-ph/9910410].

[6] A. R. Liddle and D. H. Lyth, "Cosmological Inflation and Large-Scale Structure," Cambridge University Press, Cambridge (2000).

[7] R. H. Brandenberger, "Lectures on the Theory of Cosmological Perturbations," Lect. Notes Phys. **646**, 127 (2004) [arXiv:hep-th/0306071].

[8] C. L. Bennett *et al.*, "First Year Wilkinson Microwave Anisotropy Probe (WMAP) Observations: Preliminary Maps and Basic Results," Astrophys. J. Suppl. **148**, 1 (2003) [arXiv:astro-ph/0302207].

[9] G. Hinshaw *et al.*, "Three-Year Wilkinson Microwave Anisotropy Probe (WMAP) Observations: Temperature Analysis," submitted to Astrophys. J. (2006) [arXiv:astro-ph/0603451].

[10] A. R. Liddle and D. H. Lyth, "COBE, Gravitational Waves, Inflation and Extended Inflation," Phys. Lett. **B 291**, 391 (1992) [arXiv:astro-ph/9208007].

[11] D. N. Spergel *et al.*, "First Year Wilkinson Microwave Anisotropy Probe (WMAP) Observations: Determination of Cosmological Parameters," Astrophys. J. Suppl. **148**, 175 (2003) [arXiv:astro-ph/0302209].

[12] H. V. Peiris *et al.*, "First Year Wilkinson Microwave Anisotropy Probe (WMAP) Observations: Implications for Inflation," Astrophys. J. Suppl. **148**, 213 (2003) [arXiv:astro-ph/0302225].

[13] D. N. Spergel *et al.*, "Wilkinson Microwave Anisotropy Probe (WMAP) Three Year Results: Implications for Cosmology," submitted to Astrophys. J. (2006) [arXiv:astro-ph/0603449].

[14] A. Kosowsky and M. S. Turner, "CBR Anisotropy and the Running of the Scalar Spectral Index," Phys. Rev. **D 52**, 1739 (1995) [arXiv:astro-ph/9504071].

[15] A. R. Liddle, P. Parsons, and J. D. Barrow, "Formalising the Slow-Roll Approximation in Inflation," Phys. Rev. **D 50**, 7222 (1994) [arXiv:astro-ph/9408015].

[16] A. Lewis and S. Bridle, "Cosmological Parameters from CMB and Other Data: A Monte-Carlo Approach," Phys. Rev. **D 66**, 103511 (2002) [arXiv:astro-ph/0205436].

[17] L. Page *et al.*, "Three Year Wilkinson Microwave Anisotropy Probe (WMAP) Observations: Polarization Analysis," submitted to Astrophys. J. (2006) [arXiv:astro-ph/0603450].

[18] C. L. Kuo *et al.*, "High Resolution Observations of the CMB Power Spectrum with ACBAR," Astrophys. J. **600**, 32 (2004) [arXiv:astro-ph/0212289].

[19] A. C. S. Readhead *et al.*, "Extended Mosaic Observations with the Cosmic Background Imager," Astrophys. J. **609**, 498 (2004) [arXiv:astro-ph/0402359].

[20] C. Dickinson *et al.*, "High Sensitivity Measurements of the CMB Power Spectrum with the Extended Very Small Array," Mon. Not. Roy. Astron. Soc. **353**, 732 (2004) [arXiv:astro-ph/0402498].

[21] W. J. Percival *et al.*, "Parameter Constraints for Flat Cosmologies from CMB and 2dFGRS Power Spectra," Mon. Not. Roy. Astron. Soc. **337**, 1068 (2002) [arXiv:astro-ph/0206256].

[22] M. Tegmark *et al.*, "Cosmological Parameters from SDSS and WMAP," Phys. Rev. **D 69**, 103501 (2004) [arXiv:astro-ph/0310723].

[23] L. Hoi and G. P. Holder, "The Offset Lognormal Matrix for CBI," http://www.physics.mcgill.ca/~hoiloison/cbi (2006).

[24] S. Cole *et al.*, "The 2dF Galaxy Redshift Survey: Power-Spectrum Analysis of the Final Dataset and Cosmological Implications," Mon. Not. Roy. Astron. Soc. **362**, 505 (2005) [arXiv:astro-ph/0501174].

[25] J. M. Cline and L. Hoi, "Inflationary Potential Reconstruction for a WMAP Running Power Spectrum," JCAP **0606**, 007 (2006) [arXiv:astro-ph/0603403].

[26] S. L. Bridle, A. M. Lewis, J. Weller, and G. Efstathiou, "Reconstructing the Primordial Power Spectrum," Mon. Not. Roy. Astron. Soc. **342**, L72 (2003) [arXiv:astro-ph/0302306].

[27] E. D. Stewart and D. H. Lyth, "A More Accurate Analytic Calculation of the Spectrum of Cosmological Perturbations Produced During Inflation," Phys. Lett. **B 302**, 171 (1993) [arXiv:gr-qc/9302019].

[28] E. D. Stewart and J.-O. Gong, "The Density Perturbation Power Spectrum to Second-Order Corrections in the Slow-Roll Expansion," Phys. Lett. **B 510**, 1 (2001) [arXiv:astro-ph/0101225].

[29] W. H. Kinney, "Inflation: Flow, Fixed Points and Observables to Arbitrary Order in Slow Roll," Phys. Rev. **D 66**, 083508 (2002) [arXiv:astro-ph/0206032].

[30] A. R. Liddle, "On the Inflationary Flow Equations," Phys. Rev. **D 68**, 103504 (2003) [arXiv:astro-ph/0307286].

[31] D. J. Schwarz, C. A. Terrero-Escalante, and A. A. Garcia, "Higher Order Corrections to Primordial Spectra from Cosmological Inflation," Phys. Lett. **B 517**, 243 (2001) [arXiv:astro-ph/0106020].

[32] S. M. Leach, A. R. Liddle, J. Martin, and D. J. Schwarz, "Cosmological Parameter Estimation and the Inflationary Cosmology," Phys. Rev. **D 66**, 023515 (2002) [arXiv:astro-ph/0202094].

[33] S. Habib, A. Heinen, K. Heitmann, G. Jungman, and C. Molina-Paris, "Characterizing Inflationary Perturbations: The Uniform Approximation," Phys. Rev. **D 70**, 083507 (2004) [arXiv:astro-ph/0406134].

[34] A. Makarov, "On the Accuracy of Slow-Roll Inflation Given Current Observational Constraints," Phys. Rev. **D 72** 083517 (2005) [arXiv:astro-ph/0506326].

[35] A. G. Muslimov, "On the Scalar Field Dynamics in a Spatially Flat Friedman Universe," Class. Quantum Grav. **7**, 231 (1990).

[36] D. S. Salopek and J. R. Bond, "Nonlinear Evolution of Long-Wavelength Metric Fluctuations in Inflationary Models," Phys. Rev. **D 42**, 3936 (1990).

[37] M. Cortes and A. R. Liddle, "The Consistency Equation Hierarchy in Single-Field Inflation Models," Phys. Rev. **D 73**, 083523 (2006) [arXiv:astro-ph/0603016].

[38] R. Easther, "An Inflationary Model with an Exact Perturbation Spectrum," Class. Quant. Grav. **13**, 1775 (1996) [arXiv:astro-ph/9511143].

[39] J. E. Lidsey, A. R. Liddle, E. W. Kolb, E. J. Copeland, T. Barreiro, and M. Abney, "Reconstructing the Inflaton Potential – An Overview," Rev. Mod. Phys. **69**, 373 (1997) [arXiv:astro-ph/9508078].

[40] E. J. Copeland, I. J. Grivell, E. W. Kolb, and A. R. Liddle, "On the Reliability of Inflaton Potential Reconstruction," Phys. Rev. **D 58**, 043002 (1998) [arXiv:astro-ph/9802209].

[41] R. Easther and W. H. Kinney, "Monte Carlo Reconstruction of the Inflationary Potential," Phys. Rev. **D 67**, 043511 (2003) [arXiv:astro-ph/0210345].

[42] D. J.H. Chung, G. Shiu, and M. Trodden, "Running of the Scalar Spectral Index from Inflationary Models," Phys. Rev. **D 68** 063501 (2003) [arXiv:astro-ph/0305193].

[43] H. M. Hodges and G. R. Blumenthal, "Arbitrariness of Inflationary Fluctuation Spectra," Phys. Rev. **D 42** 3329 (1990).

[44] J. J. Halliwell, "Scalar Fields in Cosmology with an Exponential Potential," Phys. Lett. **B 185**, 341 (1987).

[45] F. Lucchin and S. Matarrese, "Power-Law Inflation," Phys. Rev. **D 32**, 1316 (1985).

[46] L. M. Wang, V. F. Mukhanov, and P. J. Steinhardt, "On the Problem of Predicting Inflationary Perturbations," Phys. Lett. **B 414**, 18 (1997) [arXiv:astro-ph/9709032].

[47] J. D. Barrow, "Graduated Inflationary Universes," Phys. Lett. **B 235**, 40 (1990).

[48] J. D. Barrow and A. R. Liddle, "Perturbation Spectra from Intermediate Inflation," Phys. Rev. **D 47**, R5219 (1993) [arXiv:astro-ph/9303011].

[49] J. D. Barrow, "Exact Inflationary Universe with Potential Minima," Phys. Rev. **D 49**, 3055 (1994).

[50] W. H. Kinney, "Horizon Crossing and Inflation with Large η," Phys. Rev. **D 72**, 023515 (2005) [arXiv:gr-qc/0503017].